

## REVIEW

Cite this: *RSC Adv.*, 2015, 5, 101127

# Kaolinite properties and advances for solid acid and basic catalyst synthesis

Peter Adeniyi Alaba,<sup>a</sup> Yahaya Muhammad Sani<sup>ab</sup> and Wan Mohd Ashri Wan Daud<sup>\*a</sup>

Historically, clay mineral catalysts have found industrial applications since the early 1930s. However, inherent limitations such as impurities, porosity, low surface area and acidity hindered their wide and sustained acceptability, this is despite their economic advantages. Interestingly, the use of kaolinite as precursor in active catalyst synthesis has been a breakthrough for several industrial processes such as petrol chemistry; especially in catalytic refining and bulk chemistry. The same is also true for processes that require solid acid catalysts, catalyst support, co-catalyst or promoter application for positive environmental impact and economic viability. Therefore, this article reviews the physicochemical properties of kaolinite and their amenability to modification towards enhancing their catalytic properties. The article also discussed modification methods such as mechanochemical activation (dealumination), thermal activation, intercalation and chemical activation. With more advances in technology and long-term commitment to investments, kaolinite will become the ideal catalyst and precursor for synthesizing novel catalysts for a sustainable "greener" future.

Received 14th September 2015

Accepted 17th November 2015

DOI: 10.1039/c5ra18884a

www.rsc.org/advances

## 1. Introduction

Kaolinite is a 1 : 1 layer phyllosilicate clay mineral that makes up about 10–95% of the mineral kaolin. Its structure possesses a sheet of gibbsite-like  $\text{Al}(\text{OH})_4$  (octahedrally coordinated) and

a sheet of  $\text{SiO}_4$  tetrahedral combined with longitudinal sideline chains forming a dioctahedral structure called 1 : 1 layer phyllosilicate.<sup>1–3</sup> Fig. 1 shows the structural model of kaolinite.<sup>4</sup> Theoretically, its chemical formula is  $\text{Si}_2\text{Al}_2\text{O}_5(\text{OH})_4$  ( $\text{Al}_2\text{O}_5\text{Si}_2 \cdot 2\text{H}_2\text{O}$  or  $\text{Al}_2\text{O}_3 \cdot 2\text{SiO}_4 \cdot 2\text{H}_2\text{O}$ ).<sup>5–7</sup> Other components of kaolin includes mica and quartz as well as metal oxides such as  $\text{K}_2\text{O}$ ,  $\text{CaO}$ ,  $\text{TiO}_2$ ,  $\text{Fe}_2\text{O}_3$ ,  $\text{Na}_2\text{O}$ ,  $\text{MgO}$ ,  $\text{MnO}$ , and  $\text{P}_2\text{O}_5$  as impurities. It is a versatile hydrated aluminosilicate with a wide variety of industrial applications such as in catalysis, photocatalysis,<sup>8</sup> ion exchange,<sup>9</sup> decolorization,<sup>10–12</sup> adsorption,<sup>12,13</sup> catalyst supports

<sup>a</sup>Department of Chemical Engineering, University of Malaya, 50603 Kuala Lumpur, Malaysia. E-mail: ashri@um.edu.my; adeniyipee@live.com; ymsani@abu.edu.ng; Fax: +60 3 79675319; Tel: +60 1 126376195; +60 3 79675297

<sup>b</sup>Department of Chemical Engineering, Ahmadu Bello University, 870001 Nigeria



Peter Adeniyi Alaba was born in Kwara State, Nigeria in 1980 and carried out undergraduate at the Federal University of Technology Minna. He is currently concluded his post-graduate studies (Mphil.) at the University of Malaya under the supervision of Prof. Wan Mohd Ashri Wan Daud. He was appointed to a Graduate research assistantship at the University of Malaya in 2013 till

date. His research interests lie in rational design of tailored solid acid catalysts for efficient biofuel production, environmental engineering, CFD, and computational chemistry.



Yahaya Muhammad Sani was born and raised in Zaria, a city rich in cultural heritage & the capital of the Hausa kingdom of Zazzau in Nigeria. He received his B.Eng. Chem. Eng. from Ahmadu Bello University, the 2nd largest on the African continent (2002), MSc degrees in Biotechnology (Newcastle University, UK; 2007), & Chem. Eng. (A.B.U. Zaria; 2008) prior to obtaining a PhD from

University of Malaya, Malaysia. He joined A.B.U. Zaria in 2005 with research interest on catalysis, and renewable & sustainable energy. He is a registered Engineer certified by Council for the Regulation of Engineering, & a corporate member of the Nigerian Society of Engineers.

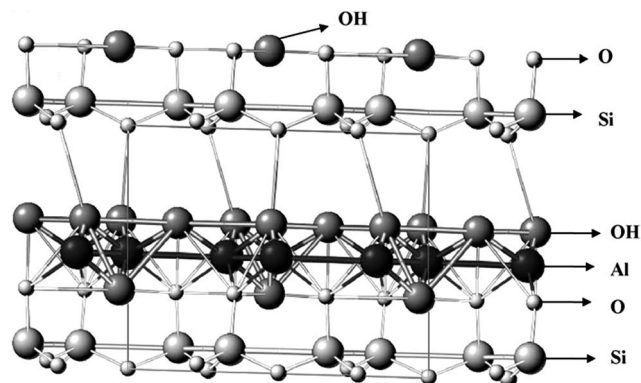


Fig. 1 Shows the structural model of kaolinite.<sup>4</sup>

and modified catalysts.<sup>14</sup> However, despite their economic advantages, kaolinite materials need to be modified because of their inherent limitations such as impurities, porosity, low surface area and acidity which hindered their wide and sustained acceptability. Modified kaolinite catalysts and supports are regaining attention in catalysis because they are naturally abundant.<sup>15,16</sup> Other favorable factors include their improved surface area, mechanical and chemical stability, and high Lewis and Brønsted acid sites density. The materials are also environmentally benign<sup>9,17</sup> with cation exchange capacity (CEC). Reactivity and surface properties have enhanced the application of kaolinite in the chemical industry based on surface modifications. There are various methods, as proposed in the open literature, for enhancing the properties of kaolinite. These include chemical activation (intercalation, alkali, organic and inorganic acid),<sup>17</sup> intercalation,<sup>18</sup> mechanochemical,<sup>19,20</sup> and thermal treatments.<sup>17,18</sup>

However, modified kaolinite have received much attention because of their crystalline structure<sup>21</sup> and large pore size, which are advantageous in the conversion of bulky molecules.<sup>22</sup>



Professor Wan Mohd Ashri Wan Daud received his bachelor degree in Chemical Engineering at Leeds University, Leeds, UK in 1991 and his master's degree in Chemical Engineering at the University of Sheffield, Sheffield, UK in 1993. He received his PhD degree in Chemical Engineering at the University of Sheffield in 1996. After nine years as an academic and scientist at the Faculty of Engineering, in 2005,

he became Professor of Chemical Engineering. Since 2005 until now, he has worked as a Professor of Chemical Engineering at the University of Malaya, Malaysia. His research fields include energy, biomass conversion to bio-fuel, catalysts synthesis, polymerization and separation processes, and hydrogen storage. He has more than 131 publications in Web Science journals.

Applying mechanochemical techniques has great effects on surface modifications, which is pronounced in Szeg and Zettlitz kaolinite. Mechanochemical activation of these materials improves their active centers, surface area, and pore volume.<sup>20,23</sup> Kaolinite materials are also amenable to alkali, organic and inorganic acid activation.

Acid and alkali treatment dissolve the external layer and eliminate impurities. Further, dealumination or desilication of kaolinite' structure changes the structural and chemical composition<sup>16</sup> of the material. Similarly, the number of acid sites, surface area and catalytic properties of amorphized kaolin (calcined or grounded), smectic clays (montmorillonite and saponite) and fibrous clays (palygorskite and saponite)<sup>19,20,22,23</sup> increases. Their wide range of pore sizes, strong acid sites and partially amorphous nature<sup>17,24</sup> facilitate the strong acidic properties of modified kaolinite catalysts. These make them viable for dehydration reactions, biomass conversion,<sup>17</sup> and catalytic cracking.<sup>10,17,25</sup> Modified kaolinite may also act as meso- and macroporous supports for transition metal oxide adsorbents or catalysts in the reacting mixture because of their partially amorphous nature. Furthermore, modification improves the effectiveness,<sup>26,28</sup> reactivity,<sup>11,28</sup> and efficiency<sup>11,30</sup> as well as stability<sup>11</sup> of the catalysts *via* increased aggregation of metal oxide.<sup>11,30</sup> Instances of such application include pollution control removal of impurities,<sup>30</sup> especially in waste water treatment<sup>11</sup> and use as a photo-Fenton catalyst.<sup>31</sup> Others include free fatty acid (FFA) esterification<sup>17</sup> and steam gasification.<sup>27</sup> Interestingly, kaolinite are impervious to microbial attack, thermally stable, hydrophilic in nature and easily regenerated. Some authors have reported the suitability of kaolinite as inorganic supports for enzymatic (organic) catalysts.<sup>31-34</sup> Furthermore, several researchers have highlighted these materials as economical precursors in synthesizing microspherical zeolitic molecular sieves such as Y and X zeolites. Evidently, zeolites are popular in fluid catalytic cracking processes.<sup>36-38</sup>

Despite extensive researches on catalytic applications of these materials, the advent of synthetic silica/alumina and zeolite Y has seemingly overshadowed their popularity. Moreover, rapidly expanding FCC units led to increased catalyst consumption. This created a dearth of high quality starting materials for *in situ* synthesis. Therefore, this review aims at exploring the physicochemical properties of kaolinite that make them suitable for catalysis. To achieve this aim seamlessly, the article reviewed the physicochemistry and how their amenability to modification enhances catalysis. The review comprises six sections: an introductory section, followed by a general discussion on physicochemical properties and modification in Section 2. Section 3 reviews the different types of modifications while Section 4 presents instances that discuss the applicability of kaolinite as a precursor in synthesizing microspherical zeolites. To stimulate further researches, Section 5 gives in-depth analyzes of kaolinite as catalyst supports while Section 6 highlights applications of these catalytic materials. The discussion concludes by proffering promising solutions that will ensure the prominence of kaolinite in catalysis. These include recent advances in improving the development of new materials.

## 2. Physicochemical properties

The physicochemical characteristics of kaolinite determine their industrial applications in catalysis. Manipulating these properties increases the industrial applicability of these materials by enhancing their activity and product selectivity.<sup>39</sup> Therefore, this section highlights how analyzes such as XRD, TGA, DSC and FTIR reveal modifications in kaolinite. The section also discusses instances in which thermal activation and surface charge heterogeneity affect these physicochemical properties. Table 1 shows the chemical composition of different kaolin samples with Si/Al ratios ranging from 1.1 to 1.78. The table also highlights impurities such as K<sub>2</sub>O, CaO, TiO<sub>2</sub>, Fe<sub>2</sub>O<sub>3</sub>, Na<sub>2</sub>O, MgO, MnO, and P<sub>2</sub>O<sub>5</sub>.

### 2.1. FTIR studies

Fourier transformed infrared (FTIR) techniques detect bonding, acidity, structural and chemical properties of kaolinite according to their vibrational mode.<sup>2,37–44</sup> Generally, kaolinite exhibit structural hydroxyl group OH stretching vibration between 3703 and 3566 cm<sup>-1</sup> and physically absorbed water is present around 1629 cm<sup>-1</sup>. The apical Si–O in-plane stretching vibration is between 1107 and 1118 cm<sup>-1</sup>, and the skeleton Si–O–Si in-plane stretching vibration is between 1014 and 1032 cm<sup>-1</sup>. The Al–OH bending vibration is between 912 and 938 cm<sup>-1</sup>, and the Al–OH translational vibration is between 695 and 796 cm<sup>-1</sup>. They also exhibit a Si–O–Al bending vibration between 536 and 541 cm<sup>-1</sup> and Si–O bending vibrations at 426 and 471 cm<sup>-1</sup>. Table 2 shows this information for different kaolinite materials.<sup>8,23,25</sup>

### 2.2. XRD studies

XRD diffractograms reveal structural defects in kaolinite because of variability in the peak positions and modulation of their intensities in kaolinite XRD patterns.<sup>7,45,46</sup> XRD identification of order/disorder is challenging because of overlapping peaks and interferences in kaolinite. The degree of structural order affects modification strategies like mechanochemical activation and intercalation as discussed in Section 3.1 and 3.2. The degree of kaolinite XRD patterns exhibit broad band

between  $2\theta = \sim 12.2\text{--}35^\circ$  with 4 peaks, which have basal spacing of about 0.71, 0.446, 0.358 and 0.256 nm, respectively.<sup>47</sup> Hinckley index (HI) measures the degree of structural order in a kaolinite's crystal structure.<sup>48</sup> Other techniques for analyzing kaolitic rocks consisting of not less than 20 wt% kaolinite include the weighting intensity ratio index (WIRI)<sup>49</sup> and the Aparicio–Galan–Ferrell index (AGFI).<sup>50,52</sup> HI values range from 0.3 to 1.8. Higher HI value indicates greater degree of structural order.<sup>51</sup> For ordered kaolinites, the HI value is greater than 1.0 while HI is below 1.0 for disordered kaolinites.<sup>45,46</sup> It is possible to obtain the HI value using the (02, 11) band which consists of the 02l and 11l sequences (20 to 23° 2θ CuK) because it is sensitive to random and interlayer displacements of type b/3 and 2.<sup>52</sup> This index value is:

$$HI = \frac{A + B}{A_h} \quad (1)$$

where  $A$  is the ( $1\bar{1}0$ ) reflection height above the band of the overlapping peak;  $B$  is the ( $11\bar{1}$ ) reflection height above the band of the overlapping peak and  $A_h$  is the overall reflection height of the ( $1\bar{1}0$ ) peak above the background as shown in Fig. 2 below.<sup>47,52</sup>

Similarly, it is appropriate to obtain the AGFI value from the (02, 11) band. Conversely, weighting peak intensity ratio of (020), ( $1\bar{1}0$ ) and ( $11\bar{1}$ ) peak reflection estimates AGFI value thus:

$$AGFI = \frac{I(1\bar{1}0) + I(11\bar{1})}{wI(020)} \quad (2)$$

For ( $1\bar{1}0$ ) and ( $11\bar{1}$ ) peak intensities ( $I_A$  and  $I_B$ ), the weighting coefficient is 1, while for (020) intensity,  $I_C$ , the weighting coefficient,  $w = 2$ . Therefore, eqn (2) is rearranged thus:

$$AGFI = \frac{I_A + I_B}{2I_C} \quad (3)$$

where  $I_A$  is the ( $1\bar{1}0$ ) peak reflection intensity,  $I_B$  is the ( $11\bar{1}$ ) peak reflection intensity and  $I_C$  is the (020) peak reflection intensity (Fig. 2). DIFPATAN (a computer program developed by Kuzel, 1991)<sup>53</sup> computes the peak intensity values for  $I_A$ ,  $I_B$  and  $I_C$  appropriately.

Table 1 Physicochemical properties of some kaolinite sample

Kaolinite sample		Si/Al	K <sub>2</sub> O (wt%)	CaO (wt%)	TiO <sub>2</sub> (wt%)	Fe <sub>2</sub> O <sub>3</sub> (wt%)	Na <sub>2</sub> O (wt%)	MgO (wt%)	MnO (wt%)	P <sub>2</sub> O <sub>5</sub> (wt%)	H <sub>2</sub> O/LOI <sup>a</sup> (wt%)	d001	Ref.
Notation	Origin												
AK	Unknown	1.20	0.9	—	0.4	0.4	—	—	—	—	—	7.202	40
FK	Brittany (F)	1.30	2.5	—	—	0.5	—	—	—	—	—	7.110	40
EK	Unknown	1.20	1	—	0.4	0.4	—	—	—	—	—	7.237	40
DK	Charentes basin (F)	1.10	0.5	0.4	0.7	0.8	—	—	—	—	—	7.231	40
MK	Mahoming, China	1.24	0.12	0.15	0.25	0.41	0.18	0.22	—	—	14.00	7.108	8
BK	Beihai, China	1.26	0.9	0.01	0.05	0.32	0.2	0.12	—	—	13.47	7.162	8
HK	Hanpu, China	1.34	1.26	0.01	0.06	0.39	0.03	0.15	—	—	12.51	7.108	8
LK	Longyan, China	1.24	0.19	0.1	0.12	0.74	0.03	0.04	0.01	—	14.68	7.108	8
KK	Zhangjiakou, China	1.30	0.01	0.47	1.38	0.4	0.08	0.01	0	0.1	13.93	7.170	41
CK	Datong, China	1.78	0.6	0.39	0.05	1.52	0.72	1.33	0.07	<0.1	11.61	7.170	41
KF	Damrec, France	1.49	0.34	0.03	0.12	0.68	0.08	0.08	—	—	12.70	7.262	41

<sup>a</sup> LOI: loss on ignition.

Table 2 Recorded FTIR vibrations assignments for kaolinite samples<sup>8,26–42</sup>

Suggested assignments	Wave numbers (cm <sup>-1</sup> )							
	MK	BK	HK	LK	AK	FK	EK	DK
Si–OH stretching vibration	3740	—	—	3739	—	—	—	—
Inner surface –OH in-phase stretching (strong) vibration	3695	3703	3701	3696	3695	3695	3696	3695
Inner surface –OH out-phase stretching (medium) vibration	3660	3650	3650	3661	3669	3669	3669	3669
Inner surface –OH stretching (strong) vibration	3622	3619	3620	3620	3619	3619	3619	3619
Inner layer water –OH vibration	—	—	—	3566	—	—	—	—
Physical absorbed water –OH vibration	1629	1624	1624	1625	—	—	—	—
Apical Si–O in-plane stretching vibration	1107	1113	1118	—	1114	1114	1114	1112
Skeleton Si–O–Si in-plane stretching vibration	1014	1031	1032	1033	1031	1031	1031	1031
Al–OH bending vibration	918	912	912	913	938	938	938	936
AL–OH (“gibbsite-like” layer) translational vibration	792	795	796	794	792	792	792	794
	755	755	754	754	755	755	756	755
	695	697	696	689	699	698	699	698
Si–O–Al bending vibration	541	538	536	538	537	539	537	537
Si–O bending vibration	471	468	469	470	469	469	469	469
	426	429	430	432	429	429	429	429

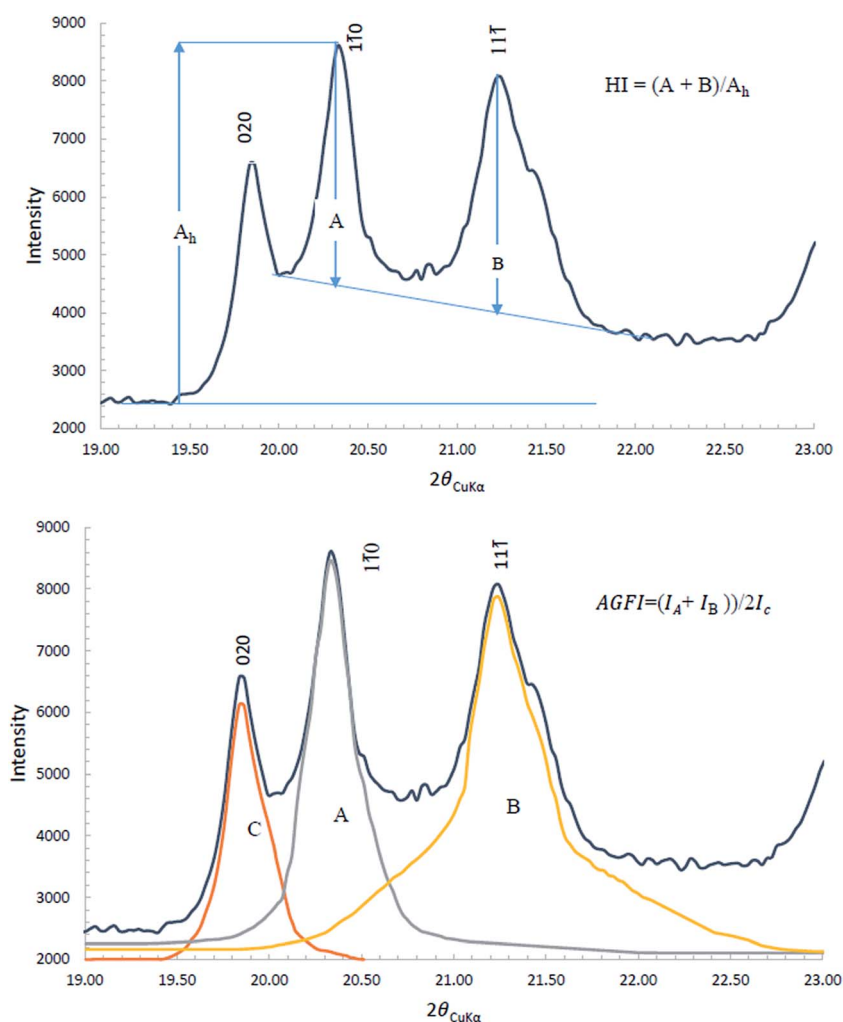


Fig. 2 Fitting procedure for HI and AGFI parameter on (02, 11) band.

WIRI is a function of the peak intensities of the (02, 11) band and full-width half maximum (FWHM) values of the corresponding (020), (110), (111) and (111) reflections resulting from decomposition of the same band. Hence, values of FWHM and corresponding intensities are obtainable from DIFPATAN.<sup>45</sup>

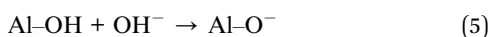
$$\text{WIRI} = 1 - e^{-\left(\frac{w_1 I(1\bar{1}0) + w_2 I(11\bar{1}) + w_3 I(1\bar{1}\bar{1})}{w_4 I(020)}\right)} \quad (4)$$

where the weighting coefficients  $w_1$ ,  $w_2$ ,  $w_3$  and  $w_4$  are the reciprocals of the FWHM values of the  $1\bar{1}0$ , (111), (111) and (020) peaks, respectively.<sup>54</sup> Chmielova *et al.*<sup>45</sup> modeled the relationship between HI and WIRI as  $\text{HI} = 0.10 + 1.44\text{WIRI}$  with  $R = 0.989$ . The relation:  $\text{AGFI} = 0.7 - 0.65\text{WIRI} + 1.86\text{WIRI}^2$  with  $R = 0.992$  provides a model relationship between AGFI and WIRI. The value of WIRI ranges between 0 and 1. For low degrees of order,  $\text{WIRI} \leq 0.4$ , for medium order,  $0.4 < \text{WIRI} \leq 0.7$  and for highly ordered  $\text{WIRI} > 0.7$ .<sup>46</sup>

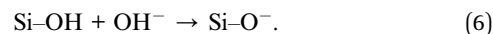
### 2.3. Surface charge heterogeneity

Hydrogen bonds bind together the tetrahedral sheets and the gibbsite-like sheets in the 1:1 layered silicate structure of kaolinite. Each bond is between an electronegative oxygen in the tetrahedral sheet and a hydroxyl group of the octahedral sheet in the *c*-axis.<sup>3</sup> Consequently, kaolinite particles possess oppositely charged surface regions in aqueous media. One charge is permanently negatively charged on the T (tetrahedral) faces, which is extremely small. This arises from minor isomorphous substitution in the tetrahedral layer. The second is a variable charge on the O faces (hydroxyl-terminated planes) because of proton donation or acceptance of the edge groups.<sup>8,55,56</sup> Depending on the pH of the protonation/deprotonation reaction in the aqueous phase, the charge on the amphoteric sites develops on the edges and faces of the octahedral (O) sheets. **This causes charge heterogeneity.<sup>55,56</sup> Protonation of aluminol groups occurs when kaolinite in aqueous medium possesses a pH below the point of zero net proton charge (PZNPC) of the main edge (amphoteric) site.** Conversely, deprotonation of silanol and aluminol groups occurs when the pH of kaolinite in aqueous medium is greater than the PZNPC of the main edge (amphoteric) site. Both gibbsite planes and broken edges of aluminol (Al-OH) sites accept protons at pH values below the PZNPC of amphoteric sites (~6.0 to 6.5). Therefore, increasing the pH above the PZNPC value results in the formation of negative charge on the gibbsite planes and broken edges, which leads to a decrease in zeta potential.<sup>8</sup> This makes the aluminum (Al-OH) groups and broken edges reactive.

Conversely, silanol (Si-OH) groups on the broken edges are only reactive at pH values above PZNPC.<sup>56</sup> However, the hydroxyl groups on the O faces are less reactive than those on the aluminol and the silanol on the broken edges.<sup>56</sup> The following reactions occur at gibbsite planes and broken edges leading to the formation of positive charges:



Similarly, the following reactions occur at gibbsite planes and broken edges leading to the formation of negative charges:



### 2.4. Electrokinetic properties

The influence of aqueous phase properties on kaolinite particle electro-osmotic permeability and zeta potential is of vital importance. Determination of the shear plane electrical potential,  $\zeta$  also known as zeta potential is essential to obtain the potential determining ions (pdi) and isoelectric point (iep). The knowledge of this properties provide a more active strategy for effecting electro-kinetic soil remediation processes. Vane and Zang<sup>57</sup> reported that the kaolinite zeta potential ranged from +0.7 mV at pH = 2 to -54 mV at pH = 10 with 0.01 M KCl ionic strength (Table 3). Further, Alkan *et al.*<sup>58</sup> studied the effect of pH, solid-liquid ratio, and concentration and type of electrolyte on the electrokinetic properties of kaolinite using the microelectrophoresis technique. The properties were tested by suspension of kaolinite in aqueous solutions of divalent heavy metal salts such as  $\text{Pb}(\text{NO}_3)_2$ ,  $\text{CuCl}_2$  and  $\text{CoCl}_2$  and mono-, di-, and trivalent salts such as, KCl, NaCl, LiCl,  $\text{NaCH}_3\text{COO}$ ,  $\text{NaNO}_3$ ,  $\text{MgCl}_2$ ,  $\text{BaCl}_2$ ,  $\text{CaCl}_2$ ,  $\text{Na}_2\text{CO}_3$ ,  $\text{AlCl}_3$ ,  $\text{Na}_2\text{SO}_4$ ,  $\text{Na}_3\text{PO}_4$ ,  $\text{FeCl}_3$ . The experimental findings of Alkan *et al.*<sup>58</sup> and Vane and Zang<sup>57</sup> are as follows:

(I) Kaolinite zeta potential and electro-osmotic permeability are strongly affected by pH, they both increase with increase in pH. This is in concomitant with the report of Wang *et al.*<sup>59</sup>

(II) The iep of kaolinite is at pH of about 2.35.

(III) Solid concentration does not significantly affect the zeta potential of kaolinite. The report of Kaya *et al.*,<sup>60</sup> also agrees with this.

(IV) Monovalent cations and anions, and di- and trivalent anions are indifferent electrolytes for kaolinite whereas  $\text{CuCl}_2$ ,  $\text{BaCl}_2$ ,  $\text{CaCl}_2$ ,  $\text{CoCl}_2$ ,  $\text{MgCl}_2$ ,  $\text{Pb}(\text{NO}_3)_2$ ,  $\text{FeCl}_3$  and  $\text{AlCl}_3$  altered the interface charge from negative to positive.

Further, the zeta potential of kaolinite is a function of its degree of structural order. A well-ordered kaolinite exhibits a lower zeta potential compared a poorly ordered one.<sup>61</sup>

### 2.5. Cation exchange capacity (CEC)

CEC quantifies the ability of kaolinite to exchange cations and retain nutrients. It informs the adsorption capacity of clay material because of its influences on the interaction with contaminants.<sup>69</sup> When a contaminants interacts with kaolinite, the charge and the mechanical properties are affected. The CEC of a sample could be determine using an ammonia-specific electrode ammonia as the exchanged cation according to the procedure suggested by Worrall.<sup>70</sup> The CEC of kaolinite depends on the pH and the amount of impurities it contains. Kaolinite material with high impurity or high pH possesses high CEC.<sup>71</sup> In addition, the CEC of kaolinite is a function of its degree of structural order. A well-ordered kaolinite exhibits a lower CEC compared a poorly ordered one.<sup>72</sup>

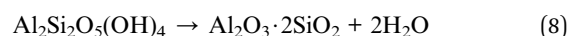
Table 3 Comparison of the reported point of zero charge (PZN) and maximum and minimum zeta potential of kaolinite

pH that creates PZN	Maximum		Minimum		Ref.
	pH	Zeta potential (mV)	pH	Zeta potential (mV)	
2 < pH < 3b	10	-54a	2	0.7a	57
4.5	11	-85	3	~8	62 <sup>a,b</sup>
	9.5	-65	3	~-3	62
<3 <sup>c</sup>	12	-32	3	Minute	63
4	11	-40	3.5	~7	64
2.2 <sup>d,e</sup>	10	-40	0	2.2	65
	11	-30	3.5	5.5	66
6	12	-40	2	10	67
	7 and 11	-25	3	-8	68 <sup>f,a</sup>
	11	-43	3	-25	68 <sup>g,b</sup>

<sup>a</sup> With 0.01 MKCL. <sup>b</sup> Georgia Kaolinite. <sup>c</sup> Steswhite kaolinite. <sup>d</sup> Lewiston, Montana. <sup>e</sup> Na kaolinite. <sup>f</sup> Low salt concentration. <sup>g</sup> 0.14 M NaCl.

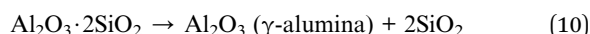
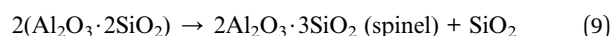
## 2.6. Thermal properties of kaolinite

Comprehensive understanding of kaolinite thermal behavior is essential to deduce the results of thermal analysis. Thermal analysis gives information on weight loss, recrystallization, decomposition and phase transformation.<sup>73</sup> Thermogravimetry/differential thermal analysis (TG/DTA) or differential scanning calorimetry (DSC) analyzes reveal the thermal behavior of the kaolinite structure.<sup>74</sup> Kaolinites exhibit two endothermic peaks (at ~55 to 80 °C and ~450 to 600 °C) and one exothermic peak (at ~980 to 1000 °C) (Fig. 3a). The first endothermic peak is of low intensity with an associated weight loss of ~0.85 wt%, which is due to water physically absorbed from the atmosphere and held within particle defects. The second endothermic peak with higher intensity is because of a weight loss of ~11.2 to 14.2 wt%.<sup>43</sup> This is due to dehydroxylation of kaolinite particles arising from interactions between OH units released from the gibbsite-like sheets.<sup>20,74,75</sup> Theoretically, the weight loss of the dehydroxylated kaolinite is 13.96 wt%.<sup>76</sup> This highlights the importance of dehydroxylation as it results in the formation of metakaolin as shown in the reaction below:



Dehydroxylation occurs simultaneously *via* homogeneous and heterogeneous mechanisms. Two neighboring OH-groups with different (less than and greater than the PZNPC) pH values interact in the homogeneous mechanism. The proton on the -OH unit with pH value less than the PZNPC reacts with one that has a pH value greater than PZNPC to release water through the interlayer spaces of the kaolinite particles. The increase in electrical conductivity at the dihydroxylation temperature<sup>74</sup> during the heterogeneous mechanism induces the migration of protons produced in the kaolinite structure to the elimination region. This enhances the interaction with the OH units and subsequent water formation. Plausibly, these explain the variations in the peak temperature. The causes of the variations include degree of structural order, pressure, water vapor partial pressure, ultrasound processing, heating rate and degree of mechanochemical activation. A higher degree of structural order produces a higher endothermic peak while a smaller particle size leads to a lower endothermic peak.<sup>8,20,74</sup>

The exothermic transformation from the endothermic peak at ~700 °C and subsequently, another exothermic peak appeared at ~980 to 1000 °C. These are attributed to transformation of metakaolin to spinel or  $\gamma$ -alumina and amorphous silica. The latter transformation starts at ~920 °C and lasts till ~1100 °C. However, the precise product obtained from this transformation is still under investigation:<sup>76</sup>



A mullite phase starts to form at ~1100 °C and increases with heating until 1300 °C. Subsequently, crystalline cristobalite emerges from the amorphous silica (eqn (12)).

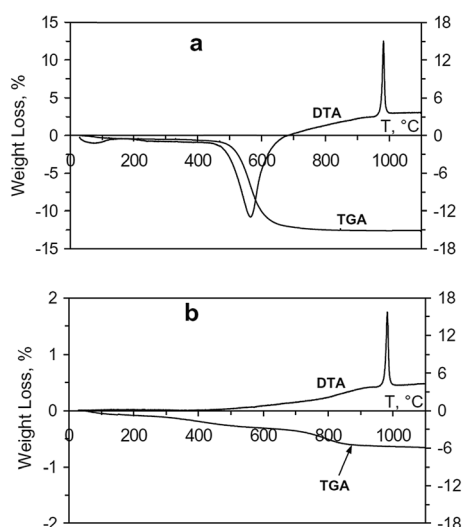
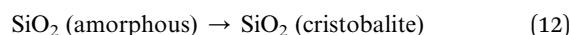
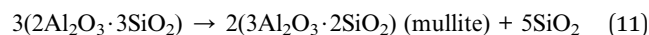


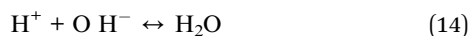
Fig. 3 TG/TDA of (a) kaolinite and (b) metakaolin.<sup>45</sup>

### 3. Modification methods

As we alluded in Section 2, manipulating the physicochemical properties of catalytic materials is one of the surest means of enhancing activity and product selectivity. Hence, this section provides specific instances on different modification methods for improving kaolinite properties such as surface area, porosity, and acidity.

#### 3.1. Mechanochemical activation

This is a modification route that entails particle size reduction and helps to increase the pore volume and surface area of kaolinite materials. It culminates in improved surface reactivity as well as a higher capacity for ion exchange.<sup>18,77</sup> Mechanochemical modification can be *via* specific micronization processes or industrial grinding.<sup>77</sup> However, mechanochemical modification leads to delamination of kaolinite particles and agglomeration of the delaminated particles to form huge spheroidal particles. The delaminated product is a randomly structured wet xerogel in which the hydroxyl units react to form coordinated water molecules attached to the active sites on the surface of the modified kaolinite. This is because of water molecule formed from the interaction between the two -OH units (eqn (14)) by proton migration in a process called prototropy.<sup>18,19</sup>



Expectedly, grinding decreases structurally ordered kaolinite that coexist with the disordered materials. This affects the degree of structural order in the delaminated precursor which determines the physicochemical properties of the mechanochemically activated kaolinite. The effect of mechanochemical activation of the kaolinite is greater for the kaolinite with high structural order compared to the kaolinite with low structural order.<sup>78</sup> Moreover, excess grinding alters kaolinite crystal structure and turns it into an amorphous material with decreased surface area and pore volume. Torres *et al.*<sup>79</sup> reported that delamination results in alumination of the kaolinite surface due to the formation of a coating of  $\text{Al}_2\text{O}_3$  generated from the grinding process. This leads to enrichment in octahedral layer of the kaolinite and a corresponding increase in the PZNPC.<sup>75</sup> Dellisanti *et al.*<sup>77</sup> reported no appreciable change until after ~5 h grinding at low spinning velocity which corresponds to 0.25 h at a high-speed spinning velocity. A bimodal particle size distribution appeared and increased appreciably with a great decrease in frequency volume (Fig. 4). This bimodal distribution after 5 h of grinding gradually transforms into a modal particle diameter after 10 to 20 h of grinding (Fig. 4). This is because of the agglomeration of delaminated particles to form huge spheroidal particles.<sup>16</sup> Dellisanti *et al.*<sup>77</sup> reported that mild grinding at low spinning velocity for 1 h does not affect the coherent scattering domain (CSD) and there is no accumulation of microstrain in the kaolinite structure. However, grinding at low spinning velocity (corresponding to 0.25 to 1 h at high-

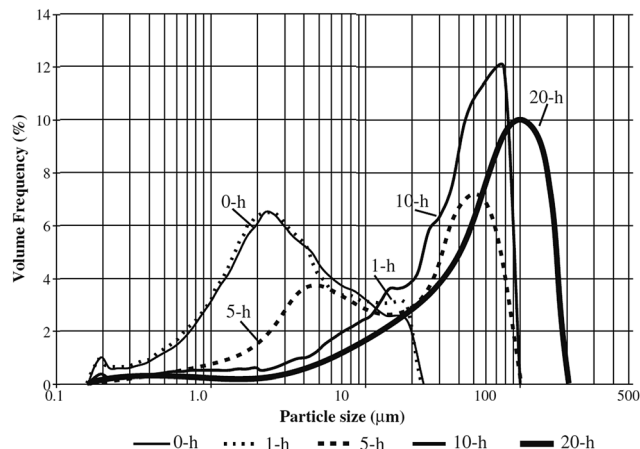


Fig. 4 Kaolinites particle size distribution before and after grinding.<sup>76</sup>

speed) for 5 to 10 h decreases the value of CSD with an associated increase in the kaolinite's microstrain structure. This is because of an increase in the FWHM value of the (001) diffraction peak resulting from a reduction in crystal size.<sup>17,77</sup> Average crystal deformation could be represented by microstrain measured along the *c*-direction (001). Further grinding above 10 h increases the amorphousness of the kaolinite structure slightly but microstrain and CSD values remain constant.<sup>76</sup> Grinding destroys the crystal structure of kaolinite by rupturing the O-H, Al-O-Si, Si-O, and Al-OH bonds<sup>80</sup> Table 2 presents kaolinite FTIR results investigated by several authors. FTIR spectral changes occur after 5 to 10 of grinding (Fig. 4). These changes include peak broadening, reduction in peak intensity and the emergence of two broadband associated with water molecules absorbed by ground samples. These bands faded or likely disappeared with increasing in grinding time.<sup>77</sup> Consequently, longer grinding time reduces surface structural variations. Further, it increases the number of acidic centers significantly. Interestingly however, further grinding of the super-active centers increases basicity.<sup>81,82</sup>

The study using mid-IR and near-IR spectroscopy also demonstrate the destruction in the kaolinite crystal structure by the rupturing of the O-H, Al-O-Si, Si-O, and Al-OH bonds. The study of Frost *et al.*<sup>83</sup> followed this destruction using near-IR spectroscopy. The intensities of the two intense characteristic bands of kaolinite at  $7065$  and  $7163 \text{ cm}^{-1}$ , which are in the spectral region of the first overtone of the hydroxyl-stretching vibration decreased upon mechanochemical activation. However, two new bands, which were assigned to the first overtone of the hydroxyl-stretching band of water emerged at  $6842$  and  $6978 \text{ cm}^{-1}$ . Concurrently, mechanochemical activation increases the intensities of the water combination bands at  $5238$  and  $5161 \text{ cm}^{-1}$ .

#### 3.2. Thermal activation

Calcination in a temperature range of  $550$  to  $950 \text{ }^\circ\text{C}$  modifies kaolinite into metakaolin. The aim of this modification route is to improve the thermal stability of the kaolinite material and prepare it for further modifications such as intercalation and chemical activation.<sup>23</sup> Also, thermal activation breaks the

hydrogen bonds between the dioctahedral layers in the 1 : 1 phyllosilicate material. This leads to evolution of the alumina coordinate towards AlVI–O, separation into aluminol-rich and silicol-rich domains and the subsequent formation of spinel phase.<sup>46,79</sup>

In the TG/DTA analysis of metakaolin exhibits only one peak. This is an exothermic peak at ~980 to 1000 °C (Fig. 3b).<sup>46</sup> However, no weight loss is associated with the exothermic peak. This is because of the germination of mullite and amorphous silica extraction from the metakaolin. The product of this synthesis is amorphous aluminosilicate which is more reactive than kaolinite. The metakaolin formed from thermal activation is a cementitious material used as a pozzolan<sup>18,47</sup> and serves as efficient starting material for chemical lixiviation.<sup>23</sup>

Vizcayno *et al.*<sup>47</sup> studied the XRD pattern of metakaolin and showed a pattern of reduced peak intensity in the 001 basal plane ( $2\theta$ ). This is due to the breakage of hydrogen bonds between the layers of kaolinite. This modification affects the basal plane peaks. Further, thermal activation at 700 °C leads to dehydroxylation of the entire moisture content of kaolinite. However, the moisture contents of the mica quartz in the solid material remain unaltered. FTIR spectra reveal the emergence of another band at ~820 cm<sup>-1</sup>. This is because of the evolution of alumina coordinate towards AlVI–O. Furthermore, the Si–O–Al bending vibration vanishes because of deformation of the 1 : 1 dioctahedral layers. This alters the Si–O and Si–O–Si stretching vibrations at ~1030, ~1039, and ~1113 cm<sup>-1</sup>.<sup>47,84,85</sup>

### 3.3. Intercalation

Intercalation is the effective insertion of a neutral polar organic substance into the interlamellar spaces of an inorganic host lattice in a regularly spaced stack to produce nano-sized composite materials. Wide interlamellar spaces prevent interactions between randomly dispersed layers in a consistent polymer matrix. This tends to facilitate exfoliation of the synthesized material. Kaolinite's unique, remarkably non-centrosymmetric structure is a suitable host for intercalation.<sup>86</sup> Factors affecting intercalation include crystallinity and the particle size of the host material. Greater crystallinity induces higher rate of intercalation while smaller particle size causes lower intercalation rate. This is because the degree of structural order declines with reduced particle size.<sup>87,88</sup> Intercalated kaolinite are efficient adsorbents,<sup>89</sup> catalysts, catalyst supports and ion exchange agents.<sup>90</sup> However, the main obstacle hindering kaolinite application as a host is the rigidity of its interlamellar space and lack of charge. Therefore, only a few guest compounds like methanol, acetamide, octadecyl amine, dimethylformamide, potassium acetate, *N*-dimethylformamide, deuterated dimethylsulfoxide and dimethylsulfoxide (DMSO) can intercalate directly into kaolinite layer. The most commonly used starting guest material is DMSO, because it possesses high thermal stability.<sup>90,91</sup> However, the obtained intercalates after introducing guest compounds could undergo further intercalation of organic guests that cannot intercalate directly.<sup>81,92</sup> Covalent grafting of small polar molecules such as DMSO or methanol achieves this modification. The guest compound

migrates to the interlamellar aluminol basal plane of the kaolinite to generate Al–O–C bonds and expand the space. Subsequently, the second guest can then displace the first guest.<sup>93</sup> Another intercalation method is co-grinding of solid organic guest and inorganic host. This method is called mechanochemical intercalation.<sup>81,75,94</sup>

Several authors<sup>81,86,87</sup> have studied kaolinite–DMSO intercalation XRD patterns. They reported the formation of kaolinite–DMSO intercalate results in a basal spacing increment of approximately 0.4 nm. The percentage DMSO intercalation is greater than 90%. This is possible because DMSO aggregates in aqueous solution and become more amorphous because of its large dipole moment. The presence of a large amount of free substratum under hydrothermal conditions results in a high rate of intercalation.<sup>90</sup> Intercalating potassium acetate (KAc) into kaolinite with DMSO as the starting guest material results in a ~0.71 nm expansion. Furthermore, two small peaks emerge at ~8.7 and ~9.8  $2\theta$ . This is because DMSO deintercalates after drying under vacuum.<sup>95–97</sup> Several FTIR spectra studies have shown the emergence of additional bands at 3663 and 905 cm<sup>-1</sup>, a reduction in the intensity of the 3696 cm<sup>-1</sup> band with no changes to the 3622 cm<sup>-1</sup> band. The 3663 cm<sup>-1</sup> band is due to the vibration of inner surface hydroxyl stretching attached to the DMSO with hydrogen bonds. Conversely, the band at 905 cm<sup>-1</sup> is due to the deformation of inner surface hydroxyl units attached to DMSO S=O units with hydrogen bonds. Vibration of the in-plane bending and out-plane bending of C–H bonds produces the 3023 and 2937 cm<sup>-1</sup> bands. However, the 3669 and 3654 cm<sup>-1</sup> bands disappear after intercalating DMSO into kaolinite. Studies have also shown subsequent disappearance of the 3663 cm<sup>-1</sup> band and emergence of bands at 3698 and 3610 cm<sup>-1</sup> when KAc is intercalated with kaolinite. Similarly, deintercalating DMSO in KAc solution leads to resurfacing of the pleochroic band at 3698 cm<sup>-1</sup>. Consequently, the presence of the 3610 cm<sup>-1</sup> band shows the successful intercalation of KAc into the kaolinite structure.<sup>90,98</sup> Table 4 presents the details of numerous FTIR assignments highlighting the effects of intercalation. Similarly, intercalating kaolinite with methanol causes space expansion of ~0.37 to 0.4 nm. This expansion is the same as the molecular diameter of methanol. This indicates the presence of methanol and weak interaction between the methanol and kaolinite. However, the percentage intercalation of methanol is ~93.7%.<sup>98</sup>

Interestingly, intercalating 1-butyl-3-methylimidazolium bromine [brmim]Br into the methanol-pretreated kaolinite increases the space expansion to ~0.7 nm.<sup>98,99</sup> There have been several studies on thermal analysis of intercalates<sup>93,98,100</sup> such as kaolinite–DMSO, kaolinite–polystyrene, and kaolinite–[bmim]Br using TG-DSC. The first weight loss similar to that of crude kaolinite appears at ~80 °C. This is because of the loss of externally absorbed water. Subsequent partial deintercalation of DMSO occurs at 190 °C while dehydrolysis of kaolinite DMSO intercalate occurs at ~479 °C.

The dehydroxylation temperature of crude kaolinite is slightly higher than that of kaolinite–DMSO. Similarly, there is partial deintercalation of 1-butyl-3-methylimidazolium bromine [brmim]Br at 277 °C followed by simultaneous decomposition



Table 4 FTIR assignments for crude kaolinite and kaolinite intercalates<sup>86,90,95,98</sup>

Suggested assignments	Wave numbers (cm <sup>-1</sup> )			
	Crude-kaolinite	Kaolinite-DSMO	Kaolinite-Kac	Kaolinite-MeOH
Inner surface -OH in-phase stretching (strong) vibration	3696	3697	3698	3700
Inner surface -OH out-phase stretching (medium) vibration	3669	3663	—	3660
Inner surface -OH stretching (strong) vibration	3622	3621	3610	3620
		3540	—	3540
		3500	—	—
In-plane bending of the vibration of C-H	—	3023	—	3031
Out-plane bending of the vibration of C-H	—	2937	—	2969
Physical absorbed water -OH vibration	1629	1635	1640	1630
Apical Si-O in-plane stretching vibration	1107	1103	—	1107
Skeleton Si-O-Si in-plane stretching vibration	1034	1032	1035	1031
Al-OH bending vibration	913	908	899	913
Al-OH (“gibbsite-like” layer) translational vibration	753	746	785	794
		695	689	692
		539	544	555
Si-O-Al bending vibration	470	467	478	469
Si-O bending vibration	431	433	438	430

of [brmim]Br and dehydroxylation of kaolinite at ~470 and 545 °C respectively. This shows the presence of stronger hydrogen bond between the kaolinite hydroxyl layer and [brmim]Br than the bond between kaolinite layers. This culminates to increase in thermal stability of the kaolinite material.<sup>98</sup> Ovramenko *et al.*<sup>101</sup> showed that combined effect of intercalation and mechanochemical activation decreases the surface acidity of kaolinite. This is because longer grinding time destroys the structural OH groups and the kaolinite structural order. This decreases the degree of intercalation and forms super-active centers on the kaolinite surface.<sup>82</sup> *In situ* decomposition of formamide bonded to these centers at 200 to 350 °C forms CO and NH<sub>3</sub>.<sup>82</sup> Hence, the significant effect that intercalation has on the acid-base properties of kaolinite super-active centers.

### 3.4. Alkali activation

Alkali activation also modifies the acidity, surface area, pore size and volume as well as the adsorption strength of the kaolinite. This makes it a suitable precursor for solid basic catalyst.<sup>102</sup> Alkali activation deprotonates aluminol and silanol groups from kaolinite materials. This leads to simultaneous dealumination and desilication of the kaolinite materials.<sup>8,103-106</sup> Alkali activation is also a suitable method for developing a variety of basic zeolites with low Si/Al ratios. These include K-F zeolite, 13X zeolite,<sup>107</sup> A, P and X zeolite,<sup>108,109</sup> zeolite N,<sup>110</sup> Na-Y zeolite,<sup>111,112</sup> MCM-41 (ref. 113) and zeolite NaA.<sup>114</sup> However, the extent of dealumination is usually low or insignificant in some instances.<sup>114,115</sup> However, Kumar *et al.*<sup>116</sup> reported that kaolinite treated with 3 M NaOH at 110 °C exhibits significant changes. These changes include 23 to 76 m<sup>2</sup> g<sup>-1</sup> surface area and 0.361 to 0.591 cm<sup>3</sup> g<sup>-1</sup> pore volume. Further, Si/Al ratio and acidity increased from 0.82 to 1.688 and 0.049 to 0.112 mmol g<sup>-1</sup> respectively. In contrast, Belver *et al.*<sup>117</sup> reported that kaolinite treated with 5 M KOH at 90 °C after calcination at 600 °C for 6 h exhibits adverse effects due to high molar concentration. The affected parameters were surface area from 18 to 4.1

m<sup>3</sup> g<sup>-1</sup>, pore volume from 80 to 7.9 cm<sup>3</sup> g<sup>-1</sup>, Si/Al ratio from 1.783 to 1.74 while acidity increased from 0.1049 to 0.1302 mmol g<sup>-1</sup>. However, 24 h treatment reduced the acidity to 0.0872 mmol g<sup>-1</sup> due to neutralization of acid sites formed as a result of excessive leaching.

Furthermore, acid activation followed by alkali activation is another technique for synthesizing ZSM-5 zeolite *via* template or template-free synthesis.<sup>118-121</sup> It is important to note that at ~1000 °C, alkali-activated kaolinite exhibit an endothermic peak while crude kaolinite exhibit exothermic peaks from ~200 to 600 °C (Fig. 5)<sup>102,121,122</sup> due to hydroxylation. The results obtained from XRD studies show a progressive decrease in the

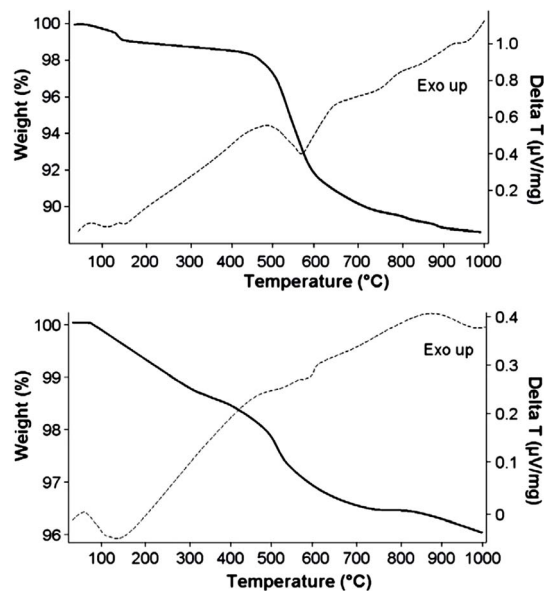


Fig. 5 TG/DTA curves of the (a) raw kaolinite and (b) samples with composition 100 Kaol, 100 SiS and, 16 NaOH, and 22H<sub>2</sub>O and cured at 80 °C for 24 h.<sup>73</sup>

peak intensity of the kaolinite structure. Similarly, FTIR studies show extreme weakness in the structural hydroxyl vibration bands of kaolinite.<sup>116</sup> The dehydroxylation is because of the deformation of some layers in the matrix of the kaolinite material. The foregoing discussion highlights the economic and structural importance of alkali activated kaolinite. The abundance of these raw materials has economical advantageous in production of zeolites compared to synthetic chemicals. Moreover, alkali-activated kaolinite has low Si/Al ratio which is a required feature for synthesizing low silica zeolites.<sup>122</sup> Since the uses of zeolites in several branches of industry have been increasing, the production of zeolites by economical ways has gained great importance in material science.

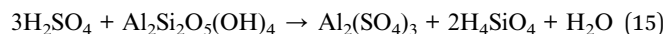
### 3.5. Acid activation

Acid-activated kaolinite are popular in adsorption and ion exchange. The activation enhances the acidity, surface area, pore size and volume, their catalytic properties of kaolinite as well as adsorption capacity.<sup>123</sup> Acid activation leads to dealumination, removal of mineral impurities, disaggregation of kaolinite particles, and external layer dissolution. This changes the structure and chemical composition of the kaolinite materials.<sup>124,125</sup> This makes it a suitable precursor for solid acid catalyst synthesis for petrochemical processes.<sup>22</sup> Aside from increasing the porosity of the kaolinite, acid activation also enhances acid centers and the surface area. Further, kaolinite is suitable as an inorganic host for intercalation and exfoliation.<sup>124</sup> Acid activation protonates aluminol (AlOH) groups using hydrogen ions from the aqueous acid medium. This leads to dealumination (eqn (15) and (16)) and increases the Si/Al ratio of the synthesis materials.<sup>8</sup> Acid activation facilitates absorption due to increase in CEC, pore volume and surface area.<sup>123,126,127</sup> This increases the amount of water physically absorbed by the kaolinite material. Conversely, activating with high concentration decreases the structural and coordinated water. This increases the endothermic peaks of the synthesized material. However, recrystallization and dehydroxylation temperature increases the endotherm peaks.<sup>25,113</sup> The endotherms are higher in kaolinite with a high degree of structural order than in those with a low degree of order.<sup>124</sup> The synthesized material is a mixture of inactivated kaolinite, amorphous and hydrous aluminosilicate as well as some partially protonated silica lamellae.<sup>106</sup> The solubility of kaolinite varies from acid to acid, the ratio of kaolinite to acid, operating temperature, leaching period, and kaolinite particle size as well as the concentration of the acid. Kaolinite solubility increases with acid concentration and leaching period, but excessive leaching leads to a decrease in its surface area.<sup>23,25</sup>

Activation with inorganic acids is more effective in generating new surface acid sites. It can also lead to collapse of the kaolinite's structure because of excessive leaching of the octahedral layer. Conversely, organic acids do not generate new acid sites as effectively as mineral acids. Meanwhile, they preserve the structure of the kaolinite because of their low activation power.

Table 5 presents a detailed comparison between organic and inorganic acid activation. It also shows the textural properties of some kaolinite samples before and after modification. Evidently, specific surface area and pore volume increase with increasing molarity of the activator and activation time. Panda *et al.*<sup>25</sup> proposed that under the same conditions, the solubility of kaolinite in HCl is less than in H<sub>2</sub>SO<sub>4</sub>. Further, the order of kaolinite solubility and subsequent increase in surface area (Table 5) attributed to acid activation is: CH<sub>3</sub>COOH < H<sub>3</sub>PO<sub>4</sub> < HCl < H<sub>2</sub>SO<sub>4</sub> < HClO<sub>4</sub> < HNO<sub>3</sub>.<sup>25,125,128</sup> Eqn (15) and (16) express the dealumination process and its effect on the Al/Si stoichiometry of kaolinite in aqueous acidic medium.

Interestingly, both organic and inorganic acids can activate kaolinite chemically.<sup>110,128–130</sup> Recently, synthesizing solid acid zeolites from kaolinite for the petrochemical industry has received great attention from numerous consortia.<sup>128–130</sup> These interests highlight the importance of acid-activated kaolinite as a zeolite precursor for converting heavy molecules.<sup>129</sup> This is because the process is cheaper and it produces zeolites with enhanced pore size and structure are more suitable than those of conventional zeolites.<sup>21</sup> However, the process requires higher calcination at ~550 to 950 °C for effective chemical activation and obtaining metakaolin from kaolinite. This is because of the presence of strong hydrogen bonds between its layers makes the material resistant to chemical attack.<sup>23,106</sup>



From XRD structural analyzes, several studies proved that all the peaks in acid-activated kaolinite correspond to the peaks of the original kaolinite material. However, acid activation reduces the kaolinite peak intensities because of the decrease in the degree of structural order. Conversely, mild acid activation increases the structural order because of an accompanying increase in crystal size which is due to decrease in the peak FWHM value. Expectedly, at higher acid concentrations, the peak in the XRD diffractograms becomes blurred. This indicates the low degree of structural order and amorphous nature of the synthesized material.<sup>22,25,124</sup>

Similarly, FTIR spectral analysis showed the inner OH stretching vibration at ~3620 cm<sup>-1</sup> has little or negligible weakness after mild acid activation. Thus, as the stronger the acid concentration, the weaker the band at 3620 cm<sup>-1</sup>. This shows that protonation increases with increasing acid concentration. It also reveals how rate of dealumination and dihydroxylation increases. However, all the bands show little or no weakness in the OH vibration bending region under mild acid activation. Increasing the acid to moderate concentrations of ~5 M reduces the bands significantly. Subsequently, all bands disappear at higher concentrations of ~10 M. This is because of the transformation of kaolinite from a crystalline phase to an amorphous phase due to the gibbsite-like layer deformation.<sup>22,25,124</sup> Moreover, Lewis site-bonded pyridines and Brønsted acid site-bonded pyridines emerge near 1446 and 1595 cm<sup>-1</sup> and at 1489, 1546 and 1633 cm<sup>-1</sup> respectively. This is due to the weakness of the H bonds on the surface of pyridine

Table 5 Textural properties of some modified kaolinites before and after activation

Kaolinite sample		Properties before activation					Activation		Properties after activation							
Notation	Origin	SSA <sup>a</sup>	Pvol <sup>b</sup>	Si/Al	Ac <sup>c</sup>	Calc <sup>d</sup> T (°C)	Chem <sup>e</sup>	Mol <sup>f</sup> (M)	Temp (°C)	Time (h)	SSA <sup>a</sup>	Pvol <sup>b</sup>	Si/Al	Ac <sup>c</sup>	Ac <sup>g</sup>	Ref
K1	Neimenggu, China	19.4	0.1	1.1			H <sub>3</sub> PO <sub>4</sub>	10	110	2	166	0.59	16.63		31	
K1	Neimenggu, China	19.4	0.1	1.1			H <sub>3</sub> PO <sub>4</sub>	5	110	2	45.3	0.17	1.76		31	
K2	Kolkata, India	23	0.361	0.65			H <sub>2</sub> SO <sub>4</sub>	10	110	4	143	1.18	8.09		25	
K2	Kolkata, India	23	0.361	0.65			H <sub>2</sub> SO <sub>4</sub>	5	110	4	107	0.967	1.63		25	
K2	Kolkata, India	23	0.361	0.65			H <sub>2</sub> SO <sub>4</sub>	3	110	4	83	0.67	1.3		25	
KGa-1b	Georgia	9.8	—				HCL	2	80	14	34.2	—			124	
KGa-2	Georgia	20.5	—				HCL	2	80	14	45	—			124	
KGa-1b	Georgia	3.8	—				H <sub>2</sub> SO <sub>4</sub>	0.25	100	3	15.6	—			9	
K3	Unknown	9	0.08			950	H <sub>2</sub> SO <sub>4</sub>	12	90	4	112	0.13		106	22	
K3	Unknown	9	0.08			850	H <sub>2</sub> SO <sub>4</sub>	12	90	20	288	0.22		114	22	
K3	Unknown	9	0.08			850	H <sub>2</sub> SO <sub>4</sub>	12	90	4	239	0.17		312	22	
K3	Unknown	9	0.08			950	H <sub>2</sub> SO <sub>4</sub>	12	90	20	110	0.13		87	22	
K4	China	—	—	2.38			NaOH	—	200	4	326	—			107	
Kflint	Para-Brazil	24	—			950	H <sub>2</sub> SO <sub>4</sub>	4	90	1	406	—		237.7	17	
Kflint	Para-Brazil	24	—			950	H <sub>2</sub> SO <sub>4</sub>	1	90	1	76	—		72	17	
Kflint	Para-Brazil	24	—			850	H <sub>2</sub> SO <sub>4</sub>	4	90	1	341	—		147.4	17	
Kflint	Para-Brazil	24	—			850	H <sub>2</sub> SO <sub>4</sub>	1	90	1	27	—		35.5	17	
K8	Jiangsu, China	41.1	—	2.00			Washing	—	—	—	41.1	—	2.00		26	
Kflint	Para-Brazil	—	—			960	HCl and 20% TPW <sup>h</sup>	0.1	200	4	—	—	5.57		30	
KC	South Africa	—	—			960	HCl and 20% TPW <sup>h</sup>	0.1	200	4	—	—	1.06		30	
KC	South Africa	—	—			960	HCl and 20% TPW <sup>h</sup>	0.5	200	4	—	—	0.901		30	
KGa-1b	Para-Brazil	12	—	1.90		950	H <sub>2</sub> SO <sub>4</sub>	4	90	1	138	—		163.4	33	
KGa-2	Para-Brazil	20	—	1.93		950	H <sub>2</sub> SO <sub>4</sub>	4	90	1	65	—		147.4	33	
Kflint	Para-Brazil	24	—	1.93		950	H <sub>2</sub> SO <sub>4</sub>	4	90	1	406	—		237.7	33	
KC	South Africa	9	—	1.96		950	H <sub>2</sub> SO <sub>4</sub>	4	90	1	233	—		250.5	33	
K5	Kolkata, India	23	0.361	0.65			H <sub>2</sub> SO <sub>4</sub>	10	110	4	143	1.18	8.09		15	
K5	Kolkata, India	23	0.361	0.65			H <sub>2</sub> SO <sub>4</sub>	5	110	4	107	0.967	1.63		15	
K5	Kolkata, India	23	0.361	0.65			H <sub>2</sub> SO <sub>4</sub>	3	110	4	83	0.67	1.3		15	
K5	Kolkata, India	23	0.361	0.65			H <sub>2</sub> SO <sub>4</sub>	1	110	4	69	0.489	0.81		15	
K6	Beijing, China	—	—	1.62			NaOH	—	—	—	364	0.47	0.57		132	
K7	Beijing, China	—	—	1.3		850	H <sub>2</sub> SO <sub>4</sub>	—	180	24	198	0.168		83	121	
K5	Kolkata, India	23	0.361	0.82	0.049	—	CH <sub>3</sub> COOH	3	110	4	38	0.504	0.885	0.11	132	
K5	Kolkata, India	23	0.361	0.82	0.049	—	H <sub>3</sub> PO <sub>4</sub>	3	110	4	42	0.658	0.972	0.11	132	
K5	Kolkata, India	23	0.361	0.82	0.049	—	HCl	3	110	4	78	1.083	1.144	0.23	132	
K5	Kolkata, India	23	0.361	0.82	0.049	—	HNO <sub>3</sub>	3	110	4	86	1.124	1.782	0.34	132	
K5	Kolkata, India	23	0.361	0.82	0.049	—	NaOH	3	110	4	76	0.591	1.688	0.11	132	
K2μm	Navalacruz, Spain	18.2	80		0.105	600	HCl	6	90	6	219		0.19		117	
K2μm	Navalacruz, Spain	18.2	80		0.105	700	HCl	6	90	6	172		0.19		117	
K2μm	Navalacruz, Spain	18.2	80		0.105	800	HCl	6	90	6	209		0.19		117	
K2μm	Navalacruz, Spain	18.2	80		0.105	900	HCl	6	90	6	50.7		0.14		117	
K2μm	Navalacruz, Spain	18.2	80		0.105	700	HCl	6	90	24	21.9		0.14		117	
K2μm	Navalacruz, Spain	18.2	80		0.105	700	KOH	1	90	6	8.5				117	
K2μm	Navalacruz, Spain	18.2	80		0.105	600	KOH	1	90	6	9.2				117	
K2μm	Navalacruz, Spain	18.2	80		0.105	700	KOH	5	90	6	3.7	8.1			117	
K2μm	Navalacruz, Spain	18.2	80		0.105	600	KOH	5	90	6	4.1	7.9		0.11	117	
K2μm	Navalacruz, Spain	18.2	80		0.105	600	KOH	6	90	24	2.4		0.09		117	

Table 5 (Contd.)

Kaolinite sample	Properties before activation				Activation		Properties after activation						Ref			
	Notation	Origin	SSA <sup>a</sup>	Pvol <sup>b</sup>	Si/Al	Ac <sup>c</sup>	Calc <sup>d</sup> T (°C)	Chem <sup>e</sup>	Mol <sup>f</sup> (M)	Temp (°C)	Time (h)	SSA <sup>a</sup>		Pvol <sup>b</sup>	Si/Al	Ac <sup>c</sup>
K10	Leghorn, Italy		17		2.02		600	HCl	2	80	4	185		16.67		131
K10	Leghorn, Italy		17		2.02		600	HCl	6	80	4	318		17.7		131
K10	Leghorn, Italy		17		2.02		600	H <sub>2</sub> SO <sub>4</sub>	1	80	4	164		4.65		131
K10	Leghorn, Italy		17		2.02		600	H <sub>2</sub> SO <sub>4</sub>	3	80	4	250		21.86		131
PBK-K	Unknown		26.6				550	H <sub>2</sub> SO <sub>4</sub>	4	100	0.75	70.4				125
PBK-K	Unknown		26.6				550	HNO <sub>3</sub>	4	100	0.75	101				125
PBK-K	Unknown		26.6				550	HClO <sub>4</sub>	4	100	0.75	79.7				125
KS 1	Ukraine		25				500	HCl	3	105	5	29.6				125
Kflint	Para-Brazil		17				850	H <sub>2</sub> SO <sub>4</sub>	4	130	0.25	187			4.32	130
Kflint	Para-Brazil		17				850	H <sub>2</sub> SO <sub>4</sub>	4	130	0.13	150			0.84	130
Kflint	Para-Brazil		17				850	H <sub>2</sub> SO <sub>4</sub>	4	130	0.25	285			1.44	130
Kflint	Para-Brazil		17				850	H <sub>2</sub> SO <sub>4</sub>	4	130	0.13	246			0.57	130
Kflint	Para-Brazil		17				950	H <sub>2</sub> SO <sub>5</sub>	4	130	0.25					130
Ka	Southwestern		19	0.103				Kaolinite-porphyrin intercalate	—	150	315	10	0.068			85

<sup>a</sup> SSA: BET specific surface area (m<sup>2</sup> g<sup>-1</sup>). <sup>b</sup> Pvol: pore volume (cm<sup>3</sup> g<sup>-1</sup>). <sup>c</sup> Ac: acidity (mmol g<sup>-1</sup>). <sup>d</sup> Calc: calcination temperature (°C). <sup>e</sup> Chem: chemical activation. <sup>f</sup> Mol: molarity (M). <sup>g</sup> Acs: acid sites (μmol g<sup>-1</sup>). <sup>h</sup> TPW: 12-Tungstophosphoric acid.

molecules.<sup>33,131</sup> Table 6 shows the XRD properties and FTIR assignments of several chemically activated kaolinite after thermal treatment.

## 4. Application of modified kaolinite

### 4.1. As catalyst support

Several attributes such as abundant availability, flexural and thermal stability, high capacity for enzymatic applications, resistance to leaching, and microbial activities have enabled kaolinite to remain relevant for over 13 decades. Further, kaolinite are eco-friendly, porous, possess small size disk (SSD) and preserve their energy and chemical functionality with prolong applications.

These features made them suitable for several industrial utilizations, most especially as catalyst supports.<sup>34,132,133</sup> Most importantly, the low cost of kaolinite has made it an economic replacement for other catalyst support in starting materials such as mullite (3Al<sub>2</sub>O<sub>3</sub>·2SiO<sub>2</sub>), alumina (Al<sub>2</sub>O<sub>3</sub>), and cordierite (2MgO·2Al<sub>2</sub>O<sub>3</sub>·5SiO<sub>2</sub>). The price of kaolinite is about 100 times lesser than that of alumina.<sup>132</sup> Also, the sintering temperature of kaolinite (~1250 °C) is less than that of alumina (~1600 °C). Besides these, kaolinite possess greater flexural strength and lower density than alumina. Kaolinite can also be blended with other materials such as dolomite, natural hydroxyapatite (bones: Ca<sub>10</sub>(PO<sub>4</sub>)<sub>6</sub>(OH)<sub>2</sub>), calcite (CaCO<sub>3</sub>) or feldspar.<sup>132</sup> Kaolinite is effective catalyst support for numerous reactions. These include zero valent Fe nanoparticles for the removal of aqueous Cu<sup>2+</sup> and Co<sup>2+</sup> ions<sup>32</sup> and bimetallic iron/nickel nanoparticles for use in waste water treatment.<sup>11</sup> Others include 12-tungstophosphoric for oleic acid esterification,<sup>30,134</sup> Cu<sup>2+</sup> and Co<sup>2+</sup> for enhanced thermal strength,<sup>135</sup> and nickel oxide for steam gasification of asphaltene.<sup>27</sup> In addition, they can support transition metals (Fe, Ni, Co and Cu) for carbon nanotubes and carbon sphere synthesis,<sup>135–137</sup> lipase for effective esterification,<sup>34</sup> chitosan, and maghemite (γ-Fe<sub>2</sub>O<sub>3</sub>).<sup>13</sup> Kaolinites also support cobalt for synthesis of 2,3-dihydrofuran,<sup>138</sup> Fe for heterogeneous Fenton-like reactions,<sup>10</sup> cobalt phosphomolybdate for decolorization of azo-stuff<sup>12</sup> and antimony doped with tin oxide (Sb–SnO<sub>2</sub>).<sup>30,139</sup> Kaolinites have rendered immense support in catalysis in improving surface area, stability in inorganic solvents, thermal, mechanical and chemical strength, aggregation, and reactivity as well as in controlling the leaching of metals, metal oxide catalysts and biocatalysts.<sup>11</sup>

It is possible to use kaolinite as a support directly or after modification by thermal or treatment or chemical activation to increase the surface area. Impregnation, co-precipitation, chemical vapor deposition (CVD), deposition, and adsorption from solution disperse the primary catalyst onto the support surface. Several factors favor catalyst dispersion onto the support. These include the crystal size of the support material, a PZNPC value of the support of less than 8, and the high ion exchange capacity of the catalyst. Others are low catalyst concentration, lower sintering temperature and competing ions in the solution.<sup>140,141</sup> Calcination enhances catalyst incorporation onto the support by transforming the support material

Table 6 Various application of modified kaolinite, XRD and FTIR analysis, number of acid sites and the conversion and yield of the reaction

Kaolinite sample		Characterization				Reaction									
Notation	Origin	Modification strategy	Mol <sup>a</sup> (M)	Time (h)	XRD	FTIR	Application	SSA <sup>b</sup> (m <sup>2</sup> g <sup>-1</sup> )	Temp. (°C)	Time (h)	Conv <sup>c</sup> (wt%)	Liquid yield (wt%)	Sel <sup>d</sup> (wt%)	Acs <sup>e</sup>	Ref.
Kflint	Para-Brazil	H <sub>2</sub> SO <sub>4</sub> activation	4	1	There is disappearance of the three well resolved peak between 20° and 24° (2θ) an emergence a broad band between 15° and 25° (2θ). This is due to the complete breakdown of the kaolinite crystalline structure and a structural water loss because of the transformation of the gibbsite-like Al <sub>2</sub> O <sub>3</sub> into penta- and tetra-coordinated Al groups		Esterification of oleic acid	408	160	4	98.9	—	237.7	17	
Kflint	Para-Brazil	H <sub>2</sub> SO <sub>4</sub> activation	4	1			Esterification of oleic acid	341	130	4	84.2		237.7	17	
Kflint	Para-Brazil	H <sub>2</sub> SO <sub>4</sub> activation	4	0.25			Esterification of oleic acid	187	100	0.5	95.2			130	
Kflint	Para-Brazil	H <sub>2</sub> SO <sub>4</sub> activation	4	0.13			Esterification of oleic acid	150	100	0.5	56.4			130	
Kflint	Para-Brazil	H <sub>2</sub> SO <sub>4</sub> activation	4	0.25			Esterification of oleic acid	285	100	0.5	83.3			130	
Kflint	Para-Brazil	H <sub>2</sub> SO <sub>4</sub> activation	4	0.13			Esterification of oleic acid	246	100	0.5	13.5			130	
K8	Jiangsu, china	Washing					Cracking	41.1	460		13.4	—	—	26	
Kflint		HCl and 20% TPW <sup>f</sup>	0.1	4	Metakaoline treated with 12-tungstophosphoric acid (HPW) shows peaks at 10.55°, 25.69° and 34.59° (2θ) confirming the presence of HPW in crystalline form	Metakaoline supported 12-tungstophosphoric acid (HPW) in aqueous medium possesses three typical absorptions at 1072 cm <sup>-1</sup> (P-O), 961 cm <sup>-1</sup> (W=O) and 884 cm <sup>-1</sup> (W-Oc-W)	Esterification of oleic acid		100	2		97.21	—	29	
KGa-1b	Georgia	H <sub>2</sub> SO <sub>4</sub> activation	4	1	All the kaolinite peaks are replaced by a broad band between 20° and 30° (2θ) that	Exhibits Lewis site-bonded pyridine near 1446 and 1595 cm <sup>-1</sup> and Brönsted	Esterification of oleic acid	138	160	4	94.8	—	163.4	32	

Table 6 (Contd.)

Kaolinite sample		Characterization			Reaction			Liquid							
Notation	Origin	Modification strategy	Mol <sup>a</sup> (M)	Time (h)	XRD	FTIR	Application	SSA <sup>b</sup> (m <sup>2</sup> g <sup>-1</sup> )	Temp. (°C)	Time (h)	Conv <sup>f</sup> (wt%)	Yield (wt%)	Sel <sup>d</sup> (wt%)	Acs <sup>e</sup>	Ref.
Kga-2	Georgia	H <sub>2</sub> SO <sub>4</sub> activation	4	1	could be attributed to an SiO <sub>2</sub> amorphous phase, and emergence of three peaks at 30°, 44° and 56° (2θ) showing a shape of type IIb	site-bonded pyridine at 1489 and 1546 cm <sup>-1</sup> as well as 1633 cm <sup>-1</sup> relating to the weak H bond to the pyridine molecules surface	Esterification of oleic acid	65	160	4	72	—	22.9	32	
Kffint	Para-Brazil	H <sub>2</sub> SO <sub>4</sub> activation	4	1	All the kaolinite peaks are replaced by a broad band between 20° and 30° (2θ) that could be attributed to an SiO <sub>2</sub> amorphous phase, and emergence of three peaks at 30°, 44° and 56° (2θ) showing a shape of type IIa	Exhibits Lewis site-bonded pyridine near at 1446 and 1595 cm <sup>-1</sup> and Brönsted site-bonded pyridine at 1489 and 1546 cm <sup>-1</sup> as well as 1633 cm <sup>-1</sup> relating to the weak H bond to the pyridine molecules surface	Esterification of oleic acid	406	160	4	98.9	—	237.7	32	
KC	South Africa	H <sub>2</sub> SO <sub>4</sub> activation	4	1	All the kaolinite peaks are replaced by a broad band between 20° and 30° (2θ) that could be attributed to an SiO <sub>2</sub> amorphous phase, and emergence of three peaks at 30°, 44° and 56° (2θ) showing a shape of type IIa	Exhibits Lewis site-bonded pyridine near at 1446 and 1595 cm <sup>-1</sup> and Brönsted site-bonded pyridine at 1489 and 1546 cm <sup>-1</sup> as well as 1633 cm <sup>-1</sup> relating to the weak H bond to the pyridine molecules surface	Esterification of oleic acid	335	160	4	98.8	—	250.5	32	
K5	Kolkata, India	No activation	10	4	XRD pattern similar to that of zeolite Y	Shows similar bands assigned to zeolite Y	Cracking of polypropylene	143	450	0.33	—	89.5	—	15	
K6	Beijing, China	NaOH activation	—	—	XRD pattern similar to that of zeolite Y	Shows similar bands assigned to zeolite Y	Cracking of heavy crude oil	364	500	—	—	74.4	37.3	141	

Table 6 (Contd.)

Kaolinite sample		Characterization				Reaction									
Notation	Origin	Modification strategy	Mol <sup>a</sup> (M)	Time (h)	XRD	FTIR	Application	SSA <sup>b</sup> (m <sup>2</sup> g <sup>-1</sup> )	Temp. (°C)	Time (h)	Conv <sup>f</sup> (wt%)	Liquid yield (wt%)	Sel <sup>d</sup> (wt%)	Acs <sup>e</sup>	Ref.
K7	Beijing, China	H <sub>2</sub> SO <sub>4</sub> activation		24	All the characteristic peaks of ZSM-5 were observed	All the bands assigned to ZSM-5 were observed	FCC naphtha aromatization	198.3	550	—	—	73.93	83	121	
K9	A1-Azraq, Jordan	HCl activation	2				Debutylation of 2- <i>tert</i> -butylphenol		230	0.5	94	25 <sup>h</sup>	128		
K9	A1-Azraq, Jordan	HCl activation	1				Debutylation of 2- <i>tert</i> -butylphenol		230	0.5	97	50 <sup>h</sup>	128		
K9	A1-Azraq, Jordan	HCl activation	0.5				Debutylation of 2- <i>tert</i> -butylphenol		230	0.5	96	28 <sup>h</sup>	128		
K9	A1-Azraq, Jordan	H <sub>3</sub> PO <sub>4</sub> activation	1				Debutylation of 2- <i>tert</i> -butylphenol		230	0.5	97	50 <sup>h</sup>	128		
K9	A1-Azraq, Jordan	CH <sub>3</sub> COOH activation	1				Debutylation of 2- <i>tert</i> -butylphenol		230	0.5	92	31 <sup>h</sup>	128		
K10	Leghorn, Italy	HCl activation	2	4			2-Propanol dehydration	185	120		26.1		132		
K10	Leghorn, Italy	HCl activation	6	4		Exhibits Lewis site-bonded at 1445 and 1596 cm <sup>-1</sup> , Bronsted site-bonded pyridine at 1547 cm <sup>-1</sup> and disappearance of all strong acid sites from the surface	2-Propanol dehydration	318	120		40.8		132		
K10	Leghorn, Italy	H <sub>2</sub> SO <sub>4</sub> activation	1	4		Exhibits Lewis site-bonded at 1454 and 1622 cm <sup>-1</sup> , Bronsted site-bonded pyridine at 1547 and 1638 cm <sup>-1</sup> , and weakly bonded hydrogen at 1597 cm <sup>-1</sup>	2-Propanol dehydration	164	120		99.4		132		
K10	Leghorn, Italy	H <sub>2</sub> SO <sub>4</sub> activation	3	4		Disappearance of all strong acid sites from the surface	2-Propanol dehydration	250	120		55.8		131		
PBK-K		H <sub>2</sub> SO <sub>4</sub> activation	4	0.75			Friedel Crafts alkylation	70.42	80	0.5	86.12	—	—	128	
PBK-K		HNO <sub>3</sub> activation	4	0.75			Friedel Crafts alkylation	100.9	80	0.5	87	—	—	128	
PBK-K		HClO <sub>4</sub> activation	4	0.75			Friedel Crafts alkylation	79.69	80	0.5	86.5	—	—	128	

Table 6 (Contd.)

Kaolinite sample		Characterization			Reaction										
Notation	Origin	Modification strategy	Mol <sup>a</sup> (M)	Time (h)	XRD	FTIR	Application	SSA <sup>b</sup> (m <sup>2</sup> g <sup>-1</sup> )	Temp. (°C)	Time (h)	Conv <sup>c</sup> (wt%)	Liquid yield (wt%)	Sel <sup>d</sup> (wt%)	ACS <sup>e</sup>	Ref.
KS 1	Ukraina	HCl activation	3	5	Patterns of the original kaolinite and its acid activated form were similar and indicating that there are no serious changes taking place in the clay structure due to mild acid activation	It exhibit the same characteristic peak with the original kaolinite due to the fact that the acid activation is so mild	Absorption 3-methoxybenzaldehyde	24.95	60	3	80	—	—	—	129
Kflint	Para-Brazil	H <sub>2</sub> SO <sub>4</sub> activation	4	0.25	There is disappearance of the peaks and emergence a broad band between 15° and 35° (2θ) attributed to the presence of amorphous SiO <sub>2</sub> phase, and three intense peak at 25.5°, 37.9° and 48.2° (2θ) due to formation of anatase or rutile TiO <sub>2</sub> usually found in accessories to kaolins in the Capim river region	Exhibits absorption bands of pyridinium ion at 1533 and 1636 cm <sup>-1</sup> due to the presence of Brønsted sites and the bands at 1448 and 1627 cm <sup>-1</sup> attributed to Lewis sites-bonded pyridine	Esterification of oleic acid	187	115	0.67	96.5	—	—	4.32	130
Kflint	Para-Brazil	H <sub>2</sub> SO <sub>4</sub> activation	4	0.13			Esterification of oleic acid	150	100	0.5	56.4	—	—	—	130
Kflint	Para-Brazil	H <sub>2</sub> SO <sub>4</sub> activation	4	0.25			Esterification of oleic acid	285	100	0.5	83.3	—	—	—	130
Kflint	Para-Brazil	H <sub>2</sub> SO <sub>4</sub> activation	4	0.13			Esterification of oleic acid	246	100	0.5	13.5	—	—	—	130
Ka	Southwestern Brazil	Kaolinite-porphyrin intercalate		315	There is disappearance of 7.14 Å peak of the kaolinite on the kaolinite basal spacing and emergence of a peak at 10.6 Å of the basal spacing of the kaolinite-porphyrin intercalate	The OH band on the kaolinite at 3618 cm <sup>-1</sup> is adjusted to 3620 cm <sup>-1</sup> and there is emergence of C-H band at 2924 and 2848 cm <sup>-1</sup>	Oxidation of cyclohexanone	10	80	24	85	100	—	—	85



Table 6 (Contd.)

Kaolinite sample		Characterization				Reaction									
Notation	Origin	Modification strategy	Mol <sup>a</sup> (M)	Time (h)	XRD	FTIR	Application	SSA <sup>b</sup> (m <sup>2</sup> g <sup>-1</sup> )	Temp. (°C)	Time (h)	Conv <sup>f</sup> (wt%)	Liquid yield (wt%)	Sel <sup>d</sup> (wt%)	Acs <sup>e</sup>	Ref.
K3			12	20			Isomerization of 1-butene	110			6.1	90.2 <sup>g</sup>	87	22	
K3	Unknown	H <sub>2</sub> SO <sub>4</sub> activation	12	20	Acid treatment of metakaolin that consists essentially of Al <sub>2</sub> O <sub>3</sub> ·2SiO <sub>2</sub> metakaolinite, led to very weak alteration in the XRPD pattern		Isomerization of 1-butene	288			18	78.78 <sup>g</sup>	114	22	
K3	Unknown	H <sub>2</sub> SO <sub>4</sub> activation	12	4			Isomerization of 1-butene	112			7.5	89.3 <sup>g</sup>	106	22	

<sup>a</sup> M: molarity (M). <sup>b</sup> SSA: BET specific surface area (m<sup>2</sup> g<sup>-1</sup>). <sup>c</sup> Conv: conversion. <sup>d</sup> Sel: selectivity. <sup>e</sup> Acs: acid sites (μmol g<sup>-1</sup>). <sup>f</sup> TPW: 12-tungstophosphoric acid activation. <sup>g</sup> Isobutene selectivity. <sup>h</sup> Debutylation selectivity.

from a crystalline phase to an amorphous phase and the catalyst becomes insoluble.<sup>31</sup>

**4.1.1. Support for fluid cracking catalyst.** Due to lower price and availability, modified kaolinite constitutes a suitable support for FCC catalysts. Fortification of FCC catalysts with modified kaolinite inculcates porosity on the catalyst structure.<sup>140</sup> This could help to improve the cracking activity towards production of gasoline with high octane number as well as enhance the yield of lower olefins such as butylene and propylene.<sup>142,143</sup> Barry *et al.*<sup>144</sup> invented a novel porous mullite *via* calcination of kaolinite at 1200 °C. They reported that the synthesized mullite were resistant to attrition due to formation of strong inter-crystalline bonds between the mullite crystals. The mullite was impregnated with a chloroplatinic acid solution by incipient wetness. The resulting catalyst was used in FCC unit for CO oxidation. Absil *et al.*<sup>143</sup> invented phosphorous modified kaolinite blended with ZSM-5 zeolites. The catalyst blend with 40 wt% of ZSM-5 and about 2.3–2.5 wt% phosphorous composition shows good attrition resistance (4–5). It was used in cracking of Joliet sour heavy gas oil in a fixed-fluidized bed unit. The catalyst blend showed significant improvement in the butylene and propylene yield compared to the base catalyst. This report corroborated with an earlier study.<sup>145</sup>

## 4.2. As stand-alone catalyst

Modified kaolinite have proved to be efficient solid catalysts and catalyst supports in various reactions. These include cracking, esterification, aromatization, alkylation, adsorption, oxidation and isomerization. This improved conversion, yield and selectivity in several reactions, as shown in Table 6 is attributed to their robust enhancement in surface area, thermal stability and acidity. It is apparent from the table that under the same activation conditions, conversion increases with increasing specific surface area.<sup>125,130</sup> However, dehydration of 2-propanol with H<sub>2</sub>SO<sub>4</sub>-treated kaolinite exhibited a contrary trend.<sup>131</sup> This is probably because of the disappearance of all of the strong acid sites from the synthesized solid acid catalyst at higher acid concentrations, despite the overall higher surface area.

**4.2.1. Synthesis of microspherical zeolitic molecular sieves.** Several studies have shown the viability of kaolinite as starting materials for synthesizing microspherical zeolitic materials. This is because they are resistant to attrition, thermally and hydrothermally stable, cheap and readily available.<sup>135,146–148</sup> A standard way of synthesizing microspheres is by mixing metakaolin (obtained from kaolinite), raw kaolinite, sodium silicate and water. A spray drying technique dries the mixture before calcination to form the required fluid microspheres. Mixing the microspheres with an aqueous solution of NaOH to form slurry enhances stirring. Hydrothermal treatment of the slurry with continuous stirring crystallizes into faujasite zeolite. Proper monitoring of the crystallization process minimizes the formation of unwanted B zeolite. The composite material synthesized from this process may be more than 15% faujasite zeolite with Si/Al ratio greater than 4. For instance, Haden *et al.*<sup>137,140</sup> and Brown *et al.*<sup>146,147</sup> have

synthesized and patented catalytic cracking catalysts such as crystalline faujasite, X and Y zeolites.

Haden *et al.*<sup>139</sup> used this procedure to synthesize 22.6% NaY zeolite with Si/Al ratio of 4.53. To improve the faujasite zeolite yield, Haden *et al.*<sup>140</sup> proposed the application of deflocculating agent to slurries of hydrated kaolin with higher levels of solids to aid spray drying. The authors separated the resulting microspheres into two (10/90) fractions by weight prior to calcination and alkali treatment. The calcination temperatures employed for the 10 and 90 fractions were below and above the clay exotherms respectively. To obtain Y zeolite with improved resistance to attrition and higher yield of 52% within shorter crystallization time, the authors posit mixing the two fractions before treating with caustic soda solution. In a recent study,<sup>148</sup> Atta *et al.* dealuminated metakaolin with inorganic acid in synthesizing X zeolite. This increased the Si/Al ratio to the expected value rather than using sodium silicate as reported by Haden *et al.*<sup>139</sup>

Interestingly, the authors obtained 57% faujasite zeolite comprised of 34% X zeolite and 23% Y zeolite. They attributed this to the similar synthesis conditions for both zeolites such as Si/Al ratio, pH value, aging, reaction temperature and time. This seems improbable because<sup>149</sup> used 22 h aging period to achieve 52% Y zeolite while<sup>146</sup> used 72 h. However, Chandrasekhar *et al.*<sup>149</sup> gave the plausible explanation. They proposed that purity and crystallinity of Y zeolite increase with longer aging periods. Hence, Haden *et al.* would have generated a higher percentage of Y zeolite if they had increased the aging period.

**4.2.2. In synthesis of silica aluminophosphate (SAPO) sieve.** SAPOs are microporous zeolitic materials with high amount of strong acidity which favor them in process such as olefins production.<sup>150–154</sup> The conventional SAPOs are synthesized hydrothermally from natural compounds containing silica, alumina and phosphorus individually or lamella aluminophosphates developed from related compounds,<sup>155–157</sup> which make them too expensive. Thermally modified raw kaolinite (metakaolin) can serve as a cheap source of both silica and alumina in synthesis of SAPO molecular sieve such as SAPO-5, SAPO-11, SAPO-20, SAPO-34, SAPO-44 and SAPO-47. This is because the silica and alumina atom in the metakaolin are capable of coordinating well with related ligands.<sup>158</sup> However, Wang *et al.*<sup>158</sup> revealed that from previous research, not all the silica and alumina atom in metakaolin partake in the development of SAPO framework. The extra framework silica and alumina constitutes impurity in SAPO, which does not favor their catalytic application. To proffer solution to this drawback, they investigated synthesis of SAPO-34 in a three steps crystallization process. The first step is transformation of kaolinite to metakaolin at 800 °C to make it active for further treatment. The second step involves transformation of the metakaolin to primary building units (PBU) by aging and initial heating. The final stage is crystallization at 150 °C. These steps produced SAPOs void of contaminate phases using kaolinite as a cheap precursor. Meanwhile, SAPOs being microporous molecular sieve with high density of acid sites, they are prone to rapid deactivation by coking, which decrease their catalytic activity.<sup>150</sup> This informs the need to develop SAPOs that are capable of coke suppression.

Recently, several author had studied synthesis of hierarchical mesoporous SAPOs with mild acidity to solve the problem of rapid deactivation.<sup>153,159–161</sup> Zhu *et al.*<sup>160</sup> synthesized hierarchical SAPO-34 composed of decussate zeolite slice units by using raw kaolin as a special silica and alumina source. The improved reactivity and selectivity of olefin in conversion dimethyl ether to olefin reaction are credited to the distinctive hierarchical network. Cui *et al.*<sup>153</sup> also reported the efficiency of hierarchical cross-like SAPO-34 developed through hydrothermal process using polyethylene glycol as the mesostructure directing agent. The catalyst performed excellently achieving up to 96% olefins selectivity, which was ascribed to ease of diffusion of both reactants and product through the well-connected pore channels.

## 5. Conclusion

Kaolinites are regaining their seemingly diminished popularity in several industrial processes, owing to the interesting physicochemical properties and other attributes. Prominent amongst the properties are surface charge heterogeneity and the degree of structural order which are usually measured by HI, AGFI or WIRI. Kaolinites are economical and environmentally benign starting materials for the synthesis of cheaper and eco-friendly catalysts, catalyst supports, ion exchange materials and adsorbents. These make them suitable supplements and in some instances, more effective substitutes for conventional materials, especially in catalysis. However, to appreciate the industrial applications of kaolinite, advances are required to enhance their properties for optimal use as highlighted in this review. Noteworthy is that mechanochemical activation improves the surface area and pore volume of kaolinite. This improves reactivity and ion exchange capacity in kaolinite materials. However, longer grinding reduces the degree of orderliness and the crystallinity of the material. Similarly, thermal activation weakens the hydrogen bonds that hold the kaolinite layers together to dehydroxylate the materials. This paves the way for effective activation. Conversely, chemical activation takes advantage of kaolinite' charge heterogeneity attributed to its amphoteric nature. This is possible with or without previous modifications such as mechanochemical and thermal activation. Acid activation improves the acidity and surface area of the catalytic material. This acidity enhancement is made possible *via* protonation of the ALOH groups which was facilitated by kaolinite surface charge heterogeneity.

Intercalation is another modification method of keen interest. Researchers are employing this in synthesizing nano-sized composite catalytic materials. These have higher performance in catalysis because they offer shorter diffusion times when compared with microporous materials. Further, intercalation does not destroy kaolinite structure compared with other activation methods. The degree of intercalation is mainly determined by the degree of structural order of the starting kaolinite. High the degree of structural order engenders high the degree of intercalation. The foregoing highlights the suitability of kaolinite as viable starting materials of choice in catalysis for synthesis of stand-alone catalysts and catalyst support which are essential in processes such as FCC, olefins production and biodiesel production.

## Acknowledgements

This study was carried out with the aid of a research grant from Fundamental Research Grant Scheme (FRGS) Grant (project no: FP031-2013A) under University of Malaya.

## References

- 1 D. M. A. Melo, J. A. C. Ruiz, M. A. F. Melo, E. V. Sobrinho and M. Schmall, *Microporous Mesoporous Mater.*, 2000, **345–349**, 38.
- 2 J. Madejova, *Vib. Spectrosc.*, 2003, **1–10**, 31.
- 3 W. Yang and A. Zaoui, *Appl. Clay Sci.*, 2013, **98–106**, 80.
- 4 D. L. Bish and R. B. Von Dreele, *Clays Clay Miner.*, 1989, **37**, 289–296.
- 5 K. Okada, A. Shimai, T. Takei, S. Hayashi, A. Yasumori and K. J. D. MacKenzie, *Microporous Mesoporous Mater.*, 1998, **289–296**, 21.
- 6 C. D. Madhusoodana, Y. Kameshima, A. Nakajima, K. Okada, T. Kogure and K. J. D. MacKenzie, *J. Colloid Interface Sci.*, 2006, **724–731**, 297.
- 7 G. Varga, *Epitoanyag*, 2007, **6–9**, 59.
- 8 P. Hu and H. Yang, *Appl. Clay Sci.*, 2013, **58–65**, 74.
- 9 K. G. Bhattacharyya and S. S. Gupta, *Desalination*, 2011, **66–75**, 272.
- 10 N. Daud and B. Hameed, *Desalination*, 2011, **291–29**, 269.
- 11 X. Liu, Z. Chen, Z. Chen, M. Megharaj and R. Naidu, *Chem. Eng. J.*, 2013, **764–771**, 223.
- 12 Q. Zhuo, H. Ma, B. Wang and L. Gu, *J. Hazard. Mater.*, 2007, **81–87**, 142.
- 13 H. Y. Zhu, R. Jiang and L. Xiao, *Appl. Clay Sci.*, 2010, **522–526**, 48.
- 14 A. Vaccari, *Catal. Today*, 1998, **53–71**, 41.
- 15 A. K. Panda and R. Singh, *J. Fuel Chem. Technol.*, 2011, **198–202**, 39.
- 16 A. Vaccari, *Appl. Clay Sci.*, 1999, **161–198**, 14.
- 17 L. A. S. do Nascimento, L. M. Z. Tito, R. S. Angélica, C. E. F. da Costa, J. R. Zamian and G. N. R. Filho, *Appl. Catal., B*, 2011, **495–503**, 101.
- 18 E. Horváth, R. L. Frost, É. Makóc, J. Kristófd and T. Cseh, *Thermochim. Acta*, 2003, **227–234**, 404.
- 19 É. Makó, Z. Senkár, J. Kristóf and V. Vágvölgyi, *J. Colloid Interface Sci.*, 2006, **362–370**, 294.
- 20 V. Vágvölgyi, J. Kovács, E. Horváth, J. Kristóf and É. Makó, *J. Colloid Interface Sci.*, 2008, **523–529**, 317.
- 21 P. Sutch and R. Young, *Clays Clay Miner.*, 1983, **357**, 31.
- 22 M. Lenarda, L. Storaro, A. Talon, E. Moretti and P. Riello, *J. Colloid Interface Sci.*, 2007, **537–543**, 311.
- 23 B. N. Dudkin, I. V. Loukhina, E. G. Avvakumov and V. P. Isupov, *Chem. Sustainable Dev.*, 2004, **327–330**, 12.
- 24 M. Hart and D. Brown, *J. Mol. Catal. A: Chem.*, 2004, **315–321**, 212.
- 25 K. P. Achyut, B. G. Mishra, D. K. Mishra and R. K. Singh, *Colloids Surf., A*, 2010, **98–104**, 363.
- 26 T. J. Rong and J. K. Xiao, *Mater. Lett.*, 2002, **297–301**, 57.
- 27 A. Hassan, F. Lopez-Linares, N. N. Nassar, L. Carbognani-Arambarri and P. Pereira-Almao, *Catal. Today*, 2013, **112–118**, 207.
- 28 B. Nandi, A. Goswami and M. Purkait, *J. Hazard. Mater.*, 2009, **387–395**, 161.
- 29 L. Shi, X. Zhang and Z. Chen, *Water Res.*, 2011, **886–892**, 45.
- 30 O. S. Lacerda Júnior, R. M. Cavalcanti, T. M. de Matos, R. S. Angélica, G. N. R. Filho and I. C. L. Barros, *Fuel*, 2013, **604–611**, 108.
- 31 O. B. Ayodele, *Appl. Clay Sci.*, 2013, **74–83**, 72.
- 32 Ç. Üzüüm, T. Shahwana, A. E. Eroğlu, K. R. Hallam, T. B. Scott and I. Lieberwirth, *Appl. Clay Sci.*, 2009, **172–181**, 43.
- 33 L. A. S. do Nascimento, R. S. Angélica, C. E. F. da Costa, J. R. Zamian and G. N. R. Filho, *Appl. Clay Sci.*, 2011, **267–273**, 51.
- 34 M. B. Abdul Rahman, S. M. Tajudin, Z. Hussein, R. Z. R. Abdul Rahman, A. Salleh and M. Basri, *Appl. Clay Sci.*, 2005, **111–116**, 29.
- 35 J. Huang, Y. Liu and X. Wang, *J. Mol. Catal. B: Enzym.*, 2008, **49–54**, 55.
- 36 B. K. Speronello, Novel zeolite fluid cracking catalysts and preparation thereof from mixtures of calcined clay, *US Pat.*, US4965233 A, 1990.
- 37 D. C. Bogert, L. B. Dight and M. A. Leskiewicz, Ultra high zeolite content FCC catalysts and method for making same from microspheres composed of a mixture of calcined kaolin clays, *US Pat.*, US5023220 A, 1991.
- 38 W. P. Hettlinger Jr, Contribution to catalytic cracking in the petroleum industry, *Appl. Clay Sci.*, 1991, **445–468**, 5.
- 39 Y. M. Sani and W. M. A. W. Daud, *Appl. Catal., A*, 2014, **140–161**, 470.
- 40 W. P. Gates, P. Komadel, J. Madejová, J. Bujdák, J. W. Stucki and R. J. Kirkpatrick, *Appl. Clay Sci.*, 2000, **257–271**, 16.
- 41 M. J. Wilson, *Clay mineralogy: spectroscopic and chemical determinative methods*, ISBN 978-94-011-0727-3, Chapman & Hall, 1994, DOI: 10.1007/978-94-011-0727-3.
- 42 M. Castellano, A. Turturro, P. Riani, T. Montanari, E. Finocchio, G. Ramis and G. Busca, *Appl. Clay Sci.*, 2010, **446–454**, 48.
- 43 C. Hongfei, J. Yang, Q. Liuc, J. Zhang and R. L. Frost, *Spectrochim. Acta, Part A*, 2010, **856–861**, 77.
- 44 C. Belver, M. A. B. Munoz and M. A. Vicente, *Chem. Mater.*, 2002, **2033–2043**, 14.
- 45 M. Chmielova and Z. Weiss, *Appl. Clay Sci.*, 2002, **65–74**, 22.
- 46 K. L. Konana, C. Peyratouta, A. Smith, J.-P. Bonnet, S. Rossignola and S. Oyetola, *J. Colloid Interface Sci.*, 2009, **103–109**, 339.
- 47 C. Vizcayno, R. M. de Gutiérrez, R. Castello, E. Rodriguez and C. E. Guerrero, *Appl. Clay Sci.*, 2010, **405–413**, 49.
- 48 Y. Hu and X. Liu, *Miner. Eng.*, 2003, **1279–1284**, 16.
- 49 A. Plancon and C. Zacharie, *Clay Miner.*, 1990, **249–260**, 25.
- 50 P. Ptáček, D. Kubátová, J. Havlica, J. Brandštetr, F. Šoukal and T. Opravil, *Thermochim. Acta*, 2010, **24–29**, 501.
- 51 L. Stoch, *Wydaw. geologiczne*, Warszawa, 1974, p. 503.
- 52 P. Aparicio and E. Galan, *Clays Clay Miner.*, 1999, **12–27**, 47.
- 53 M. Valášková, M. Riedera, V. Matějka, P. Čapková and A. Sliva, *Appl. Clay Sci.*, 2007, **108–118**, 35.
- 54 P. Ptáček, T. Opravil, F. Šoukal, J. Wasserbauer, J. Másilko and J. Baráček, *J. Eur. Ceram. Soc.*, 2013, **2793–2799**, 33.

- 55 E. Tombacz and M. Szekeres, *Appl. Clay Sci.*, 2006, **105–124**, 34.
- 56 P. V. Brady, R. T. Cygan and K. L. Nagy, *J. Colloid Interface Sci.*, 1996, **356–364**, 183.
- 57 L. M. Vane and G. M. Zang, *J. Hazard. Mater.*, 1997, **55**, 1–22.
- 58 M. Alkan, O. Demirbas and M. Dogan, *Microporous Mesoporous Mater.*, 2005, **83**, 51–59.
- 59 J.-Y. Wang, X.-J. Huang, J. C. M. Kao and O. Stabnikova, *J. Hazard. Mater.*, 2007, **144**, 292–299.
- 60 A. Kaya, A. H. Ören and Y. Yükselen, *Mar. Georesour. Geotechnol.*, 2006, **24**(3), 203–218.
- 61 G. Tari, I. Bobos, C. S. F. Gomes and J. M. F. Ferreira, *J. Colloid Interface Sci.*, 1999, **210**, 360–366.
- 62 Y. Hotta, T. Banno, Y. Nomura, S. Sano and K. Oda, *J. Ceram. Soc. Jpn.*, 1999, **107**(1249), 868–871.
- 63 L. J. West and D. L. Stewart, Effect of zeta potential on soil electrokinesis, in *The Proc. of Geoenvironment 2000*, ASCE Special Publication, 1995, pp. 1535–1549.
- 64 P. N. Lorenz, *Clays Clay Miner.*, 1969, **17**, 223–231.
- 65 R. W. Smith and Y. Narimatsu, *Miner. Eng.*, 1993, **6**, 753–763.
- 66 D. J. A. Williams and K. P. Williams, *J. Colloid Interface Sci.*, 1978, **65**, 79–87.
- 67 J. M. Dzenitis, *Environ. Sci. Technol.*, 1997, **37**, 1191–1197.
- 68 E. A. Stephan and G. G. Chase, *Sep. Purif. Technol.*, 2001, **21**, 219–226.
- 69 K. H. Tan, *Principles of Soil Chemistry*, Marcel Dekker, New York, 1982.
- 70 W. C. Worrall, *Clays and Ceramic Raw Materials*, Applied Science Pub., London, 1975, p. 203.
- 71 J. C. Miranda-Trevino and C. A. Coles, *Appl. Clay Sci.*, 2003, **23**, 133–139.
- 72 G. Tari, I. Bobos, C. S. F. Gomes and J. M. F. Ferreira, *J. Colloid Interface Sci.*, 1999, **210**, 360–366.
- 73 F. Hussin, M. K. Aroua and W. M. A. W. Daud, *Chem. Eng. J.*, 2011, **90–106**, 170.
- 74 H. Cheng, Q. Liu, J. Yang, S. Ma and R. L. Frost, *Thermochim. Acta*, 2012, **1–13**, 545.
- 75 E. Gasparini, S. C. Tarantino, P. Ghigna, M. P. Riccardi, E. I. Cedillo-González, C. Siligardi and M. Zema, *Appl. Clay Sci.*, 2013, **417–425**, 80.
- 76 A. Ghorbel, M. Fourati and J. Bouaziz, *Mater. Chem. Phys.*, 2008, **876–885**, 112.
- 77 F. Dellisanti and G. Valdre, *Int. J. Miner. Process.*, 2012, **69–77**, 102.
- 78 G. Tari, I. Bobos, C. S. F. Gomes and J. M. F. Ferreira, *J. Colloid Interface Sci.*, 1999, **210**, 360–366.
- 79 S. R. Torres, E. Basaldella and J. Marco, *J. Colloid Interface Sci.*, 1999, **339–344**, 215.
- 80 E. Mako, R. L. Frost, J. Kristof and E. Horvath, *J. Colloid Interface Sci.*, 2001, **244**, 359–364.
- 81 D. Sun, B. Li, Y. Li, C. Yu, B. Zhang and H. Fei, *Mater. Res. Bull.*, 2011, **101–104**, 46.
- 82 E. Horvath, J. Kristof, R. L. Frost, E. Mako, E. Jakab and A. Redey, *J. Colloid Interface Sci.*, 2005, **132–138**, 289.
- 83 R. L. Frost, É. Mako, J. Kristo and J. T. Klopogge, *Spectrochim. Acta, Part A*, 2002, **58**, 2849–2859.
- 84 A. Tironi, M. A. Trezza, E. F. Irassar and A. N. Scian, *Procedia Mater. Sci.*, 2012, **343–350**, 1.
- 85 N. Bizaia, E. H. de Faria, G. P. Ricci, P. S. Calefi, E. J. Nassar, K. A. D. F. Castro, S. Nakagaki, K. J. Ciuffi, R. Trujillano, M. A. Vicente, A. Gil and S. A. Korili, *ACS Appl. Mater. Interfaces*, 2009, **2667–2678**, 1.
- 86 T. A. Elbokl and C. Detellier, *J. Phys. Chem. Solids*, 2006, **950–955**, 67.
- 87 K. Song, X. Wang, P. Qian, C. Zhang and Q. Zhang, *Comput. Theor. Chem.*, 2013, **72–80**, 1020.
- 88 Y. Deng, G. N. White and J. B. Dixon, *J. Colloid Interface Sci.*, 2002, **379–393**, 250.
- 89 R. R. Da Silva and D. L. Guerra, *J. Chil. Chem. Soc.*, 2013, **1678–1683**, 58.
- 90 P. C. Lopes, F. A. Dias and L. da Silva, *Mater. Lett.*, 2003, **3397–3401**, 57.
- 91 J. Matusik, Z. Kłapyta and Z. Olejniczak, *Appl. Clay Sci.*, 2013, **426–432**, 83.
- 92 J. Matusik and Z. Kłapyta, *Science*, 2013, **433–440**, 83.
- 93 S. Letaief, I. K. Tonle, T. Diaco and C. Detellier, *Appl. Clay Sci.*, 2008, **95–101**, 42.
- 94 É. Makó, J. Kristóf, E. Horváth and V. Vágvölgyi, *Appl. Clay Sci.*, 2013, **24–31**, 83.
- 95 B. Zhang, Y. Li, X. Pan, X. Jia and X. Wang, *J. Phys. Chem. Solids*, 2007, **135–142**, 68.
- 96 C. Johnston and D. Stone, *Clays Clay Miner.*, 1990, **121–128**, 38.
- 97 H. Cheng, Q. Liu, J. Yang, X. Du and R. L. Frost, *Appl. Clay Sci.*, 2010, **476–480**, 50.
- 98 L. Zhang, C. Wang, Z. Yan, X. Wu, Y. Wang, D. Meng and H. Xie, *Appl. Clay Sci.*, 2013, **106–110**, 86.
- 99 S. Letaief and C. Detellier, *J. Mater. Chem.*, 2007, **1476–1484**, 17.
- 100 T. A. Elbokl and C. Detellier, *J. Colloid Interface Sci.*, 2008, **338–348**, 323.
- 101 N. A. Ovramenko, O. F. Zakharchenko and F. D. Ovcharenko, *Kolloidnyj Zhurnal*, 1994, **410–12**, 56.
- 102 F. Slaty, H. Khoury, J. Wastiels and H. Rahier, *Appl. Clay Sci.*, 2013, **120–125**, 75–76.
- 103 A. M. Rashad, *Construct. Build. Mater.*, 2013, **751–765**, 41.
- 104 A. M. Rashad, *Construct. Build. Mater.*, 2013, **303–318**, 41.
- 105 A. Poulesquen, F. Frizon and D. Lambertin, *Rheological Behavior of Alkali-Activated Metakaolin During Geopolymerization*, Springer, 2013, pp. 225–238.
- 106 Q. Tan, X. Bao, T. Song, Y. Fan, G. Shi, B. Shen, C. Liu and X. Gao, *J. Catal.*, 2007, **69–79**, 251.
- 107 Y. Ma, C. Yan, A. Alshameri, X. Qiu, C. Zhou and D. Li, *Adv. Powder Technol.*, 2014, **495–499**, 25.
- 108 C. Belviso, F. Cavalcante, A. Lettino and S. Fiore, *Appl. Clay Sci.*, 2013, **162–168**, 80.
- 109 M. Murat, A. Amokrane, J. P. Bastide and L. Montanaro, *Clay Miner.*, 1992, **27**, 119–130.
- 110 I. D. Mackinnon, G. J. Millar and W. Stolz, *Appl. Clay Sci.*, 2012, **1–7**, 58.
- 111 D. M. EL-Mekkawi and M. M. Selim, *J. Environ. Chem. Eng.*, 2014, **723–730**, 2.

- 112 P. A. Alaba, Y. M. Sani and W. M. A. W. Daud, *Chin. J. Catal.*, 2015, **36**, 1846–1851.
- 113 E. Du, S. Yu, L. Zuo, J. Zhang, X. Huang and Y. Wang, *Appl. Clay Sci.*, 2011, **94–101**, 51.
- 114 A. R. Loiola, J. C. R. A. Andrade, J. M. Sasaki and L. R. D. da Silva, *J. Colloid Interface Sci.*, 2012, **34–39**, 367.
- 115 D. Serrano and P. Pizarro, *Chem. Soc. Rev.*, 2013, **4004–4035**, 42.
- 116 S. Kumar, A. K. Panda and R. Singh, *Bull. Chem. React. Eng. Catal.*, 2013, **61–69**, 8.
- 117 C. Belver, M. A. B. Munoz and M. A. Vicente, *Chem. Mater.*, 2002, **2033–2043**, 14.
- 118 P. A. Alaba, Y. M. Sani, I. Y. Mohammed, Y. A. Abakr and W. M. A. W. Daud, *J. Taiwan Inst. Chem. Eng.*, 2015, 1–8, DOI: 10.1016/j.jtice.2015.09.006.
- 119 F. Pan, X. Lu, Y. Wang, S. Chen, T. Wang and Y. Yan, *Microporous Mesoporous Mater.*, 2014, **134–140**, 184.
- 120 F. Pan, X. Lu, Y. Wang, S. Chen, T. Wang and Y. Yan, *Mater. Lett.*, 2014, **5–8**, 115.
- 121 P. Wang, B. Shen, D. Shen, T. Peng and J. Gao, *Catal. Commun.*, 2007, **1452–1456**, 8.
- 122 M. Alkan, Ç. Hopa, Z. Yilmaz and H. Güler, *Microporous Mesoporous Mater.*, 2005, **176–184**, 86.
- 123 K. G. Bhattacharyya and S. S. Gupta, *Colloids Surf., A*, 2006, **277**, 191–200.
- 124 M. Valášková, K. Barabaszová, M. Hundáková, M. Ritz and E. Plevová, *Appl. Clay Sci.*, 2011, **70–76**, 54.
- 125 K. R. Sabu, R. Sukumar, R. Rekha and M. Lalithambik, *Catal. Today*, 1999, **321–326**, 49.
- 126 K. G. Bhattacharyya and S. S. Gupta, *Ind. Eng. Chem. Res.*, 2007, **46**, 3734–3742.
- 127 K. G. Bhattacharyya and S. S. Gupta, *Chem. Eng. J.*, 2008, **136**, 1–13.
- 128 S. Mahmoud and S. Saleh, *Clays Clay Miner.*, 1999, **481–486**, 47.
- 129 B. Shen, P. Wang, Z. Yi, W. Zhang, X. Tong, Y. Liu, Q. Guo, J. Gao and C. Xu, *Energy Fuels*, 2009, **60–64**, 23.
- 130 A. D. N. de Oliveira, L. R. D. S. Costa, L. H. D. O. Pires, L. A. S. do Nascimento, R. S. Angélica, C. E. F. da Costa, J. R. Zamian and G. N. D. R. Filho, *Fuel*, 2012, **626–631**, 103.
- 131 M. Perissinotto, M. Lenarda, L. Storaro and R. Ganzerla, *J. Mol. Catal. A: Chem.*, 1997, **103–109**, 121.
- 132 Y. F. Chang, S. N. Vaughn, L. R. M. Martens, J. W. Sprinkle and I. N. Walker, Molecular sieve catalyst composition, its making and use in conversion processes, WO2004060559 A1, 2004.
- 133 E. H. de Faria, G. P. Ricci, L. Marcal, E. J. Nassar, M. A. Vicente, R. Trujillano, A. Gil, S. A. Korili, K. J. Ciuffi and P. S. Calefi, *Catal. Today*, 2012, **187**, 135–149.
- 134 Y.-F. Chang, S. N. Vaughn, K. R. Clem, L. R. Martens and W. Hu, Molecular sieve catalyst composition, its making and use in conversion processes, *US Pat.*, US7241713 B2, 2007.
- 135 Y. F. Chang, Molecular sieve catalyst composition, its making and use in conversion processes, WO2006083423 A1, 2006.
- 136 A. Kovo, O. Hernandez and S. Holmes, *J. Mater. Chem.*, 2009, **6207–6212**, 19.
- 137 F. J. Dzierzanowski and W. L. Haden Jr, *US Pat.*, US3433587 A, 1969.
- 138 W. L. Haden Jr and F. J. Dzierzanowski, Zeolitic catalyst and preparation, *US Pat.*, 3,663,165, 1972.
- 139 W. L. Haden, Microspherical zeolitic molecular sieve composite catalyst and preparation thereof, *US Pat.*, US3506594 A, 1970.
- 140 W. L. Haden, Microspherical zeolitic molecular sieve composite catalyst and preparation thereof, *US Pat.*, US3647718 A, 1972.
- 141 M. C. D Jose and R. de Janeiro, *US Pat.*, 5,082,815, 1992.
- 142 S. C. S. Joseph, E. W. Albers and G. R. Wilson, *US Pat.*, 5,739,072, 1998.
- 143 A. P. L. Robert and K. A. Jocelyn, *US Pat.*, 5,366,948, 1994.
- 144 S. K. Barry, *US Pat.*, 4,628,042, 1986.
- 145 A. P. L. Robert and J. A. Herbst, *US Pat.*, 5,231,064, 1993.
- 146 S. M. Brown and G. M. Woltermann, *US Pat.*, US4157375 A, 1979.
- 147 S. M. Brown and G. M. Woltermann, *US Pat.*, US4235753 A, 1980.
- 148 A. Atta, O. Ajayi and S. Adefila, *J. Appl. Sci. Res.*, 2007, **1017–1021**, 3.
- 149 S. Chandrasekhar and P. Pramada, *Appl. Clay Sci.*, 2004, **187–198**, 27.
- 150 W. Pengfei, L. Ailing, H. Jie, X. Jing'an and L. Guanzhong, *Ind. Eng. Chem. Res.*, 2011, **9989–9997**, 50.
- 151 H. Q. Zhou, W. Yao, F. Wei, D. Z. Wang and Z. W. Wang, *Appl. Catal., A*, 2008, **112**, 341.
- 152 F. Niloufar, S. Morteza, S. J. Royaei and S. Mirarefin, *Chem. Eng. Res. Des.*, 2011, **811–816**, 89.
- 153 Y. Cui, Q. Zhang, J. He, Y. Wang and F. Wei, *Particuology*, 2013, **468–474**, 11.
- 154 T. N. Ali, F. Shohreh, S. Morteza and S. Maede, *J. Ind. Eng. Chem.*, 2012, **29–37**, 18.
- 155 Z. M. Yan, B. H. Chen and Y. Huang, *Solid State Nucl. Magn. Reson.*, 2009, **49**, 35.
- 156 H. O. Pastore, G. A. V. Martins, M. Strauss, L. G. Pedroni, G. B. Superti, E. C. de Oliveira, G. Gatti and L. Marchese, *Microporous Mesoporous Mater.*, 2008, **81**, 107.
- 157 H. O. Pastore, E. C. de Oliveira, G. B. Superti, G. Gatti and L. Marchese, *J. Phys. Chem. C*, 2007, **3116**, 111.
- 158 T. Wang, L. Xuchen and Y. Yan, *Microporous Mesoporous Mater.*, 2010, **138–147**, 136.
- 159 Y. Seung-Tae, K. Ji-Ye, C. Ho-Jeong, K. Min, J. Soon-Yong and A. Wha-Seung, *Mater. Res. Bull.*, 2012, **3888–3892**, 47.
- 160 J. Zhu, Y. Cui, Y. Wang and F. Wei, *Chem. Commun.*, 2009, 3282–3284.
- 161 L. Chen, R. W. Wang, S. Ding, B. B. Liu, H. Xia, Z. T. Zhang, *et al.*, *Chemical Journal of Chinese Universities*, 2010, **1693–1696**, 31.